Journal Pre-proof

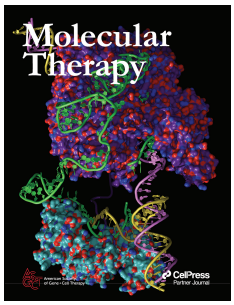

Nuclear AGO2 promotes myocardial remodeling by activating ANKRD1 transcription in failing hearts

Rong Xie, MD, Shuai Yuan, MD, PhD, Guo Hu, MD, Jiabing Zhan, MD, PhD, Kunying Jin, MD, PhD, Yuyan Tang, MD, PhD, Jiahui Fan, MD, PhD, Yanru Zhao, MD, PhD, Feng Wang, MD, PhD, Chen Chen, MD, PhD, Dao Wen Wang, MD, PhD, Huaping Li, MD, PhD

PII: S1525-0016(24)00159-X

DOI: https://doi.org/10.1016/j.ymthe.2024.03.018

Reference: YMTHE 6361

To appear in: *Molecular Therapy*

Received Date: 13 October 2023

Accepted Date: 8 March 2024

Please cite this article as: Xie R, Yuan S, Hu G, Zhan J, Jin K, Tang Y, Fan J, Zhao Y, Wang F, Chen C, Wang DW, Li H, Nuclear AGO2 promotes myocardial remodeling by activating ANKRD1 transcription in failing hearts, *Molecular Therapy* (2024), doi: https://doi.org/10.1016/j.ymthe.2024.03.018.

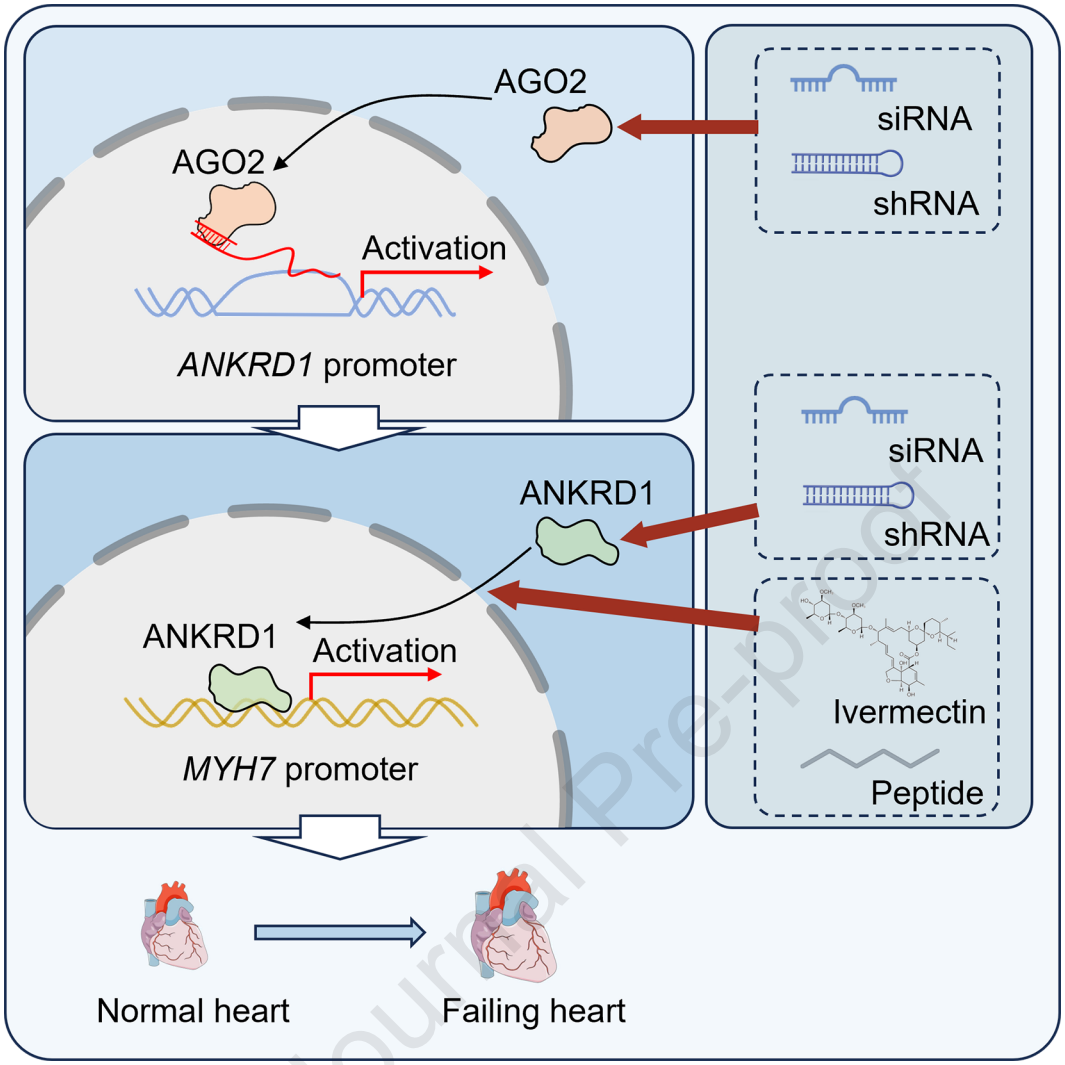

Nuclear AGO2 promotes myocardial remodeling by activating ANKRD1 transcription in failing hearts

Rong Xie[1,2#], MD; Shuai Yuan[1,2#], MD, PhD; Guo Hu[1,2], MD; Jiabing Zhan[1,2], MD, PhD; Kunying Jin[1,2], MD, PhD; Yuyan Tang[1,2], MD, PhD; Jiahui Fan[1,2], MD, PhD; Yanru Zhao[1,2], MD, PhD; Feng Wang[1,2], MD, PhD; Chen Chen[1,2]*, MD, PhD; Dao Wen Wang[1,2]*, MD, PhD, and Huaping Li[1,2]*, MD, PhD.

[1]Division of Cardiology, Tongji Hospital, Tongji Medical College, Huazhong University of Science and Technology, Wuhan 430030, China.

[2]Hubei Key Laboratory of Genetics and Molecular Mechanisms of Cardiological Disorders, Wuhan 430030, China.

*Corresponding authors: Huaping Li (email: lhp@tjh.tjmu.edu.cn), Chen Chen (email: chenchen@tjh.tjmu.edu.cn) and Dao Wen Wang (dwwang@tjh.tjmu.edu.cn). Division of Cardiology, Department of Internal Medicine, Tongji Hospital, Tongji Medical College, Huazhong University of Science & Technology, 1095# Jiefang Ave., Wuhan 430030, China. Tel/fax: 86-27-6937-8422.

[#]Rong Xie and Shuai Yuan equally contributed to this work.

Short title: nuclear AGO2 and heart failure

Abstract

Heart failure (HF) is manifested by transcriptional and post-transcriptional reprogramming of critical genes. Multiple studies have revealed that microRNAs could translocate into subcellular organelles such as nucleus to modify gene expression. However, the functional property of subcellular Argonaute2 (AGO2), the core member of the microRNA machinery, has remained elusive in HF. AGO2 was found to be localized in both cytoplasm and nucleus of cardiomyocytes, and robustly increased in failing hearts of patients and animal models. We demonstrated nuclear AGO2 rather than cytosolic AGO2 overexpression by recombinant adeno-associated virus (serotype 9) with cardiomyocyte-specific troponin T promoter exacerbated the cardiac dysfunction in transverse aortic constriction (TAC)-operated mice. Mechanistically, nuclear AGO2 activates the transcription of *ANKRD1*, encoding Ankyrin repeat domain-containing protein 1 (ANKRD1), which also has a dual function in the cytoplasm as part of I-band of the sarcomere and in the nucleus as a transcriptional cofactor. Overexpression of nuclear ANKRD1 recaptured some key features of cardiac remodeling by inducing pathological *MYH7* activation, whereas cytosolic ANKRD1 seemed cardio-protective. For clinical practice, we found ivermectin, an anti-parasite drug, and ANPep, a ANKRD1 nuclear location signal mimetic peptide, were able to prevent ANKRD1 nuclear import, resulting in the improvement of cardiac performance in TAC-induced HF.

Introduction

Chronic heart failure (CHF) is a complex clinical syndrome that results from various structural or functional impairment of ventricular filling or ejection of blood[1]. The prevalence of heart failure (HF) is increasing worldwide because of an increasing incidence related to population aging, rising prevalence of poorly controlled risk factors (i.e., hypertension, diabetes, and obesity), and prolonged survival of patients with HF due to implementation of evidence-based treatments[2]. Even with the development of comprehensive disease-modifying pharmacological therapies (e.g. ARNI, β blocker, MRA, and SGLT2 inhibitor), ~20-30% of patients diagnosed with HF still die in 5 year.[3] Therefore, new targets and mechanisms underlying HF are urgently needed.

The onset of HF is typically preceded by cardiac compensatory hypertrophy, an adaptive response to maintain cardiac function. However, in settings of sustained stress and as time progresses, cardiac hypertrophy becomes maladaptive, which ultimately transits to HF[4]. Pathological hypertrophy of adult heart is associated with *MYH6* downregulation and *MYH7* induction, which represents a reprogram to a fetal state of myosin heavy chain (MHC) expression[5]. β-MHC (also known as myosin heavy chain 7, MYH7) encoded by *MYH7* is characterized by lower adenosine triphosphatase activity and lower filament sliding velocity, but can generate cross-bridge force with a higher economy of energy consumption than α-MHC (also known as myosin heavy chain 6, MYH6) encoded by *MYH6*[6,7]. Transgenic mice replacing normally predominant α-MHC with β-MHC appears disadvantageous to the animals under severe cardiovascular stress[8]. Interestingly, a myosin heavy-chain-associated lncRNA (Mhrt) was reported to inhibit the pathological switch from MYH6 to MYH7, thereby protecting the heart from decompensated hypertrophy and failure[9]. Thus, strategies to

confine MYH7 expression may represent a therapeutic strategy against HF.

microRNAs (miRNAs) are a class of small (≈22 nt) non-coding RNAs with well-established functions in cardiovascular diseases, which negatively regulate gene expression at posttranscriptional levels in the cytoplasm. Interestingly, recent observations from our groups and others suggest that miRNAs can translocate into the nucleus and mitochondria to regulate gene expression in a positive fashion at the transcriptional or translational level[10-12]. However, for clinical practice, targeting subcellular localized miRNAs seems difficult because miRNAs are normally localized in different cellular compartments, and up to now, the mechanism underlying miRNA targeting to specific subcellular compartments translocation has remained unidentified[13,14]. In sharp contrast, signals for subcellular localization of proteins are well defined[15,16]. This promotes us to test whether targeting Argonaute2 (AGO2), the core component of miRNA-RISC (miRNA-induced Silencing Complex) machinery, in different cellular compartments might prevent the progression of cardiovascular disorders. The AGO2-containing RISC machinery typically suppresses gene expression at posttranscriptional levels in the cytoplasm, but increasing evidence reveals the presence of AGO2 in the nucleus, as well as in mitochondria[12,17-19]. Despite its clear rearrangement in various diseases[10,18], it has remained largely elusive about how subcellular AGO2 contributes to specific cardiovascular disorders, such as HF.

In this study, we reported the upregulation of AGO2 in the failing heart of pressure-overload mice, as well as in patients with HF. We found that upregulated AGO2 in nucleus could efficiently enhance *ANKRD1* transcription. Increased Ankyrin repeat domain-containing protein 1 (ANKRD1), encoded by *ANKRD1* further acts to induce the pathological activation of *MYH7*, which ultimately leads to cardiac remodeling. We demonstrated that shRNA against AGO2 or ANKRD1 delivered by recombinant adeno-

associated virus (rAAV) and blockage of ANKRD1 nuclear import by ivermectin or peptide can potently rescue TAC-induced cardiac dysfunction, suggesting a potential therapy for HF.

Results

Upregulation of AGO2 in cardiomyocytes of failing hearts

Our previous work revealed the upregulation of cardiac AGO2 in TAC-induced HF mice[20]. To further look into the mechanism, we evaluated the nuclear and cytosolic AGO2 expression by cell fractionation. The isolated nucleus was free of contamination as indicated by the lack of cytosolic protein GAPDH while the nuclear specific protein Lamin B1 was absent from the cytosolic fraction (Fig. 1A). Using these purified cellular fractions, we found that AGO2 was increased in both nucleus and cytoplasm in hearts of TAC-induced HF mice (Fig. 1A and 1B). According to the single-cell sequencing data, AGO2 is predominantly expressed in cardiomyocytes compared with fibroblasts, endothelial cells and macrophages in hearts[21]. Thus, we isolated adult mouse cardiomyocytes using Langendorff perfusion apparatus, and performed immunofluorescence of AGO2 with cardiomyocyte marker, α-actinin, indicating that both nuclear and cytosolic AGO2 were elevated in cardiomyocytes of TAC-induced failing hearts compared to Sham (Fig. 1C). Fractionation on cardiomyocytes followed by Western blotting revealed that cytosol and nuclear AGO2 were increased in cardiomyocytes while decreased in non-cardiomyocytes under TAC stress (Fig. S1). In failing hearts from patients with dilated cardiomyopathy (DCM), we also detected dramatic upregulation of both nuclear and cytosolic AGO2 (Fig. 1D and 1E). These data demonstrate the induction of AGO2 during the progression of HF.

Elevated nuclear AGO2 impairs cardiac performance in TAC-operated mice

To investigate the functional relevance of increased AGO2 in HF, we first knocked down AGO2 in cardiomyocytes using shRNA expressed from a cardiomyocyte-specific troponin T (tnt) promoter delivered by recombinant adeno-associated virus serotype 9

(rAAV9-tnt). As expected, rAAV9-shAGO2 decreased AGO2 level in hearts (Fig. 2A). Under TAC surgery, cardiac function was dramatically improved upon AGO2 inhibition (Fig. 2B and 2C). Furthermore, Hematoxylin and eosin (HE) and Sirius Red staining of heart sections indicated that rAAV-shAGO2 treatment decreased cardiac myocyte size and fibrosis in TAC-treated mice (Fig. 2D and 2E). Importantly, we did not observe any differences in control mice (Fig. S2), indicating the effect of AGO2 on the heart was only manifested under stress conditions.

We then asked whether nuclear or cytoplasmic AGO2 played a pivotal role in TAC-induced cardiac dysfunction. We engineered the nuclear and cytosolic form of AGO2 by fusing FLAG-tagged AGO2 to a nuclear localization signal (NLS) or nuclear export signal (NES), and used adenovirus (Ad) to express such nuclear or cytosolic form of AGO2 in highly purified neonatal rat ventricular myocytes (NRVMs) (Fig. S3). The immunofluorescence assay indicated that the localization signal could efficiently guide AGO2 into nucleus or cytoplasm (Fig. S4). Then, we employed rAAV9 combined with tnt promoter to express nuclear and cytosolic form of AGO2 in mice one week after TAC surgery and the mice were subjected to echo analysis eight weeks after TAC. Using these vectors, we demonstrated that overexpression of nuclear AGO2 overexpression exacerbated cardiac dysfunction and increased cardiac myocyte size and fibrosis in TAC-operated mice (Fig. 2F-I, and S5). In sharp contrast, the cytosolic form of AGO2 failed to show any detectable effects (Fig. 2F-I), despite the successful induction of AGO2 in the cytoplasm of cardiomyocytes (Fig. 2J). Again, we did not observe significant differences in control mice overexpressing either nuclear or cytosolic AGO2 (Fig. S6). Collectively, these results strongly suggested that nuclear AGO2 was directly involved in TAC-induced cardiac dysfunction.

To determine whether nuclear AGO2 acts in the compensation phase, we

overexpressed nuclear AGO2 by injecting rAAV9 into mice two weeks before TAC surgery and performed echo analysis at different time points after TAC surgery (Fig. S7). Results showed that the EF value of nuclear AGO2 overexpressed group decreased significantly while GFP group was still preserved at 2 weeks after TAC surgery, which indicated an earlier enter into cardiac decompensation phase for mice treated with nuclear AGO2. Moreover, we observed similar regulation pattern of nuclear AGO2 on cardiac performance in female mice under TAC (Fig. S8)

ANKRD1 as a direct target of nuclear AGO2 in TAC-operated mice

A previous study demonstrated that chromatin-associated RNA binding proteins (RBPs), including AGO2 were pervasive at gene promoters, indicating the ability to directly regulate transcription[22,23]. Therefore, we overexpressed nuclear AGO2 in AC16 cell line and conducted RNA-seq to identify the direct targets of nuclear AGO2 (fold change > 2, $p < 0.05$) (Fig. 3A). We intersected genes regulated by nuclear AGO2 with those remarkably upregulated or downregulated in failing hearts of TAC mice to identify potential targets of nuclear AGO2 that may directly contribute to HF. Next, we performed CUT&Tag assay using anti-FLAG antibody in AC16 cells expressing FLAG-tagged nuclear AGO2 to evaluate the distribution of AGO2 binding sites in chromatin. A total of 54,611,958 clean reads were obtained, which reach a mapping rate of 96.73%. After removing the sequences aligned to mitochondria from the aligned reads, peak calling software MACS2 was used to perform peak scanning across the entire genome to obtain information about the position and length of the peaks. A total of 25,263 peaks were obtained, and analysis revealed that approximately 32.41% peaks were located in the promoter region, which indicated transcriptional regulatory role of AGO2 (Fig. S9A and S9B). MAME software was used to identify enriched motifs in

the CUT&TAG data, and the most significant three motifs were listed in Figure S9C. Then we investigated the direct downstream targets of nuclear AGO2 that had pathophysiologic significance by integrating the mRNA-seq, LC-MS and CUT&Tag data (Fig. 3A). Through this screening strategy, two specific genes were found to meet the three requirements, including *Ankrd1* and *C3*. We detected clear binding of AGO2 on promoter region of *ANKRD1* and *C3*, suggesting the involvement in transcriptional regulation of *ANKRD1* and *C3* (Fig. 3B), which was further validated by ChIP-qPCR (Fig. 3C). A step further, we performed Western blotting on heart tissues isolated from mice treated with rAAV-AGO2-NLS or rAAV-AGO2-NES, finding that only ANKRD1 was potently upregulated after TAC surgery and was further induced by nuclear AGO2 (Fig. 3D and 3E). In contrast, C3 were not affected by nuclear AGO2 in vivo. These data suggested that ANKRD1 rather than C3 was the potential target of nuclear AGO2 in HF. To further confirm whether ANKRD1 was the direct target, we extracted highly purified NRVMs and observed similar results that ANKRD1 protein was exclusively induced by nuclear AGO2 but not cytosolic AGO2 (Fig. 3F and 3G). Consistently, global AGO2 knockdown in NRVMs by siRNAs was able to decrease ANKRD1 expression (Fig. 3H and 3I). Collectively, these results indicate that ANKRD1 is the direct target of nuclear AGO2 in TAC-induced HF.

Nuclear AGO2 acts as a transcriptional cofactor to enhance ANKRD1 transcription

Having demonstrated that ANKRD1 was a target of nuclear AGO2 in HF, we next asked how AGO2 was able to enhance *ANKRD1* transcription in the nucleus. Considering that AGO2 showed binding signals on gene promoter, we wondered whether AGO2 might function as a transcriptional cofactor and performed luciferase

198 reporter assays. As expected, luciferase reporter assays revealed the promoter activity
199 of *ANKRD1* was enhanced by AGO2 overexpression (Fig. 4A and 4B).

200 Considering that AGO2 contains RNA-binding domain rather than DNA-binding
201 domain, we tried to determine whether AGO2 targeted ANKRD1 promoter DNA via
202 nascent RNA. By using Actinomycin D, which blocked RNA synthesis, we found that
203 AGO2 binding on the *Ankrd1* promoter DNA was largely attenuated, suggesting the
204 RNA-mediated association of AGO2 with the promoter (Fig. 4C). This prompted us to
205 test whether promoter-proximal transcripts (PATs) were involved. By 5' and 3' rapid
206 amplification of cDNA ends (RACE), we demonstrated the expression of both sense
207 and antisense PATs transcribed from the promoter region of mouse *Ankrd1* (Fig. 4D).
208 By using antisense oligonucleotides (ASOs) against these PATs in both sense and
209 antisense orientation, we found that block of the *Ankrd1* sense PAT but not antisense
210 PAT prevented AGO2 binding on the *Ankrd1* promoter (Fig. 4E). RNA
211 Immunoprecipitation (RIP) followed by quantitative PCR assay also revealed direct
212 association of AGO2 with the sense PAT of *Ankrd1* rather than antisense PAT (Fig. 4F).

213 Considering that AGO2 is typically involved in miRNA-mediated gene regulation,
214 we then asked whether miRNAs were participated in AGO2 binding on the *Ankrd1*
215 sense PAT. We previously performed miRNAs-microarray on subcellular fractions of
216 cardiomyocytes, revealing that a specific cluster of miRNAs that were relatively
217 enriched in the nucleus compared to the cytoplasm[24]. Base-paring prediction by
218 RNAhybrid database suggested that out of those nuclear enriched miRNAs, a specific
219 miRNA, miR-92a-3p, was able to target both human and mouse *ANKRD1* sense PATs
220 (Fig. 4G). Furthermore, miR-92a-3p inhibition decreased AGO2 ChIP signals on the
221 *Ankrd1* promoter (Fig. 4H). RIP assay further indicated that miR-92a-3p inhibition
222 suppressed AGO2 binding on the *Ankrd1* sense PAT (Fig. 4I). These data suggest that

with the base-paring information provided by miR-92a-3p, *Ankrd1* sense PAT recruited nuclear AGO2 to *Ankrd1* promoter DNA to enhance *Ankrd1* transcription (Fig. 4J).

Nuclear AGO2 exacerbated TAC-induced cardiac dysfunction via ANKRD1

ANKRD1 is present in the I-band region of the sarcomere as a member of the titin-N2A mechanosensory unit[25], but also acts as a transcriptional cofactor in the nucleus in response to mechanical stretch[26]. To establish the functional connection between nuclear AGO2 and its target *ANKRD1*, we evaluated whether AGO2 aggravated cardiac dysfunction by modulating *ANKRD1* expression on a TAC model transduced with rAAV-tnt vectors. Eight weeks after TAC surgery, we confirmed the efficiency of nuclear AGO2 overexpression and *Ankrd1* knockdown in the heart of TAC-induced HF mice (Fig. 5A and S10). rAAV-AGO2-NLS treatment clearly exacerbated cardiac dysfunction in TAC-operated mice (Fig. 5B and 5C), whereas *Ankrd1* knockdown diminished rAAV-AGO2-NLS-induced cardiac dysfunction (Fig. 5B and 5C). Consistently, we observed coordinated changes in cardiac myocytes area and fibrosis under different treatment conditions (Fig. 5D and 5E). Collectively, these data demonstrated that overexpression of nuclear AGO2 exacerbated cardiac dysfunction in TAC mice and the adverse effects were rescuable by suppressing *Ankrd1*.

Opposite roles of nuclear ANKRD1 and cytosolic ANKRD1 in TAC-operated mice

By cell fractionation followed by Western blotting analysis, we observed that ANKRD1 was mainly presented in the nucleus with a less extent in the cytoplasm, although both increased by nuclear AGO2 overexpression (Fig. 5F). To separate the role of nuclear ANKRD1 from cytosolic ANKRD1, we engineered nuclear and cytosolic form of FLAG-tagged ANKRD1 by fusing it to NLS or NES, and confirmed

their similar expression efficiency (Fig. S11). We found that the nuclear form of ANKRD1 exacerbated cardiac dysfunction in TAC-operated mice, whereas the cytosolic ANKRD1 appeared to show some protective effects on cardiac performance (Fig. 5G and 5H). Moreover, the protective effect of AGO2 knockdown was diminished upon overexpression of nuclear, but not cytosolic, ANKRD1 (Fig. 5G and 5H). These data suggest that AGO2 exacerbated TAC-induced cardiac dysfunction mainly through enhancing the expression of nuclear ANKRD1.

Nuclear ANKRD1 induced pathological MYH7 expression in TAC-operated mice

To identify potential targets of nuclear ANKRD1, we performed RNA-seq on heart tissues from Sham and TAC mice and identified approximately 800 differentially expressed genes (fold change > 1.5, $p < 0.05$), among which 20 upregulated genes and 42 downregulated genes were further regulated by overexpression of nuclear ANKRD1 (Fig. 6A). Furthermore, LC-MS confirmed the presence of 10 upregulated and 16 downregulated genes in failing hearts (fold change > 1.2, $p < 0.05$), among which *Myh7* and *Ces1d* were dysregulated in hearts from TAC-operated mice at protein levels (Fig. 6A). Next, we conducted western blotting assay and found that only MYH7 was regulated at the protein level by overexpression of nuclear ANKRD1 (Fig. 6B and 6C). Considering TAC- and nuclear ANKRD1-induced MYH7 expression was detected at both mRNA and protein levels, we tested whether MYH6, another isoform of the myosin heavy chain, was also regulated by ANKRD1. We observed no change in the protein level of MYH6 (Fig. 6B and 6C). Anyhow, the MYH7/MYH6 ratio was clearly increased in hearts of TAC-operated mice, which was amplified by overexpression of nuclear ANKRD1 (Fig. 6C). According to published studies, adult cardiomyocytes predominately express MYH6, while embryonic cardiomyocytes predominately

express MYH7. Various cardiac stresses trigger the transition of cardiomyocytes from MYH6 to MYH7 expression[27-29]. Importantly, this shift was not just a marker of cardiac remodeling because researchers have found that MYH7 impaired systolic function of cardiomyocytes and accelerated TAC-induced cardiac hypertrophy[8,30]. Moreover, to further establish the direct activation of ANKRD1 on *MYH7* transcription, we constructed a pGL3 plasmid harboring the *MYH7* promoter. Overexpression of ANKRD1 enhanced the fluorescence signal of pGL3-MYH7 (Fig. 6D), and we further confirmed direct ANKRD1 binding with ChIP-PCR and ChIP-seq (Fig. 6E and 6F). Collectively, these data revealed the mechanism underlying nuclear AGO2-mediated ANKRD1 activation to promote cardiac remodeling (Fig. 6G).

Ivermectin and ANKRD1 NLS mimetic peptide suppressed ANKRD1 nuclear import and improved cardiac performance in TAC-operated mice

Though global *Ankrd1* knockdown by shRNA protected against TAC-induced cardiac dysfunction, ANKRD1 overexpression in nucleus and cytoplasm resulted in opposite outcomes. Based on this observation, it may present a promising therapeutic strategy for HF by blocking ANKRD1 nuclear import. Several molecules have been previously identified as inhibitors of protein nuclear import [31,32], among which a drug called ivermectin has been extensively applied in humans as a drug against parasites. We thus evaluated whether ivermectin was able to prevent the nuclear translocation of ANKRD1. Strikingly, nuclear import of ANKRD1 was suppressed and cardiac dysfunction was improved in ivermectin-treated TAC mice (Fig. 7A-D). Interestingly, the decrease of nuclear ANKRD1 was more dramatic than the increase of cytosol ANKRD1 (Fig. 7C and 7D), indicating the decrease of ANKRD1 overall level. Interestingly, we noticed that AGO2 nuclear transport was also compromised by

298 ivermectin treatment (Fig. S12). Therefore, ivermectin appears to be able to target both
299 AGO2 and ANKRD1 in the AGO2-ANKRD1-MYH7 axis. In vitro study also showed
300 nuclear ANKRD1 level was decreased by ivermectin treatment under isoproterenol
301 (ISO) stimulation (Fig. 7E and 7F). Moreover, ISO-induced cardiomyocytes
302 hypertrophy was largely abolished by ivermectin treatment (Fig. 7G). Importantly,
303 ivermectin lost these effects in ANKRD1 knockdown NRVMs (Fig. 7H). These data
304 demonstrated that ivermectin could prevent ANKRD1 nuclear import to protect against
305 cardiac hypertrophy.

306 Considering ivermectin was a global importin inhibitor, we constructed a soluble
307 cell-penetrating peptide, here called ANPep, bearing the NLS of ANKRD1 to
308 competitively inhibit ANKRD1 nuclear import. To increase the specificity of the
309 peptide, we extended the NLS sequence to 19 amino acids (mouse ANKRD1, aa85-103,
310 EDLEIIVQLKKRKKYKKTK). A cell penetrating sequence (YGRKKRRQRRR) was
311 placed at the N-terminal to help the peptide cross the cell membrane. As expected,
312 ANPep remarkably improved TAC-induced cardiac dysfunction (Fig. 7I), and nuclear
313 ANKRD1 level was decreased by ANPep administration (Fig. 7J). These data
314 suggested that ANPep could be a potential therapy specifically targeting ANKRD1
315 nuclear import for the treatment of HF in humans.

Discussion

Our results demonstrate that nuclear AGO2 was upregulated in pressure overload-induced failing hearts, which acts in the nucleus to enhance *ANKRD1* transcription. ANKRD1 had double-faces that its cytosolic form is present in I-band region of the sarcomere whereas the nucleus form induces pathological MYH7 activation and cardiac remodeling (Fig. 6G). Importantly, we show that AGO2 knockdown, ANKRD1 knockdown and blockage of the ANKRD1 nuclear import is able to effectively rescue cardiac dysfunction in TAC-induced HF.

The mechanism underlying the nuclear import of AGO2

AGO2 has been found in the nuclei of various tumor cells such as HeLa, MCF-7 and A549 cells as well as in non-tumor cells such as WI38 fibroblasts, neuronal cells and primary cardiomyocytes[10,18,19,33,34], indicating that AGO2 can be a nuclear-cytoplasmic shuttling protein. However, human tissues analysis reveals that AGO2 exhibits primarily as a nuclear protein in skin, normal cervix and cervical cancer tissues, but not in larynx, indicating that the subcellular distribution of AGO2 occurs in a cell-type and tissue context-dependent manner[35]. Mechanistically, AGO2 appears to be imported into the nucleus via nuclear transport importins. An experimentally determined protein-protein interactions database HitPredict[36] reveals direct interaction between AGO2 and nuclear transporters, such as IPO4, IPO8 and IPO9. Consistently, upon IPO8 knockdown, the localization of AGO2 is shifted from nucleus to cytoplasm in HeLa and HEK293 cells[19]. Whether IPO8 is also responsible for AGO2 nuclear import in cardiomyocytes or other mammalian cells awaits further investigation. Moreover, a NLS seems to localized in the 275-288aa (MKRKYR) of AGO2 predicted by the SeqNLS database[37], although the functional significance of this potential NLS remains to be demonstrated.

The mechanism of nuclear AGO2 in transcription control

In mammals, nuclear AGO2 is implicated in key events such as transcriptional regulation mediated by miRNAs, chromatin remodeling, and alternative RNA splicing[10,18,38-41]. It's intriguing to ask how nuclear AGO2 activates transcription at genomic loci. Previous work demonstrates that AGO2 serves as a promoter-specific platform to recruit a unique set of proteins including CTR9 to form a small activating RNAs (saRNA)-induced transcriptional activation (RITA) complex in prostate cancer PC-3 cell line[40]. CTR9 is a component of PAF1C, which is required for phosphorylation of Ser2 of RNAP II CTD that may play a role in the transition between early and productive transcription elongation[42]. However, CTR9 was neither detectable in mouse heart by LC-MS (data not shown) nor in human heart by ISH (the human protein atlas database). Instead, by AGO2 immunoprecipitation followed by LC-MS analysis specifically in mouse heart, we identified an array of proteins associated with nuclear AGO2 (data not shown) including YY1, a transcription factor. YY1 can bind to enhancers and promoter-proximal elements to form dimers and promote DNA interactions, contributing to the regulation of gene expression[43]. It's possible that AGO2, by directly interacting with YY1, facilitates ANKRD1 enhancer-promoter looping and activates gene expression. Interestingly, we observe clear binding events of H3K27ac, marker for activated enhancers on upstream region of ANKRD1 genomic loci (Fig. S13 from ENCODE database). The hypothesis that AGO2 could activate genes transcription through the interaction with YY1 to facilitate enhancer-promoter looping is an intriguing subject for future study.

Previously, we have reported that AGO2 upregulated miR-320 level by decreasing the decay rate of miR-320. As the decay of miRNAs commonly occurs in cytosol[44,45], AGO2 mediated miR-320 decay is more likely to be mediated by cytosol localized

AGO2 rather than nuclear AGO2. Since miR-320 decay was mostly likely mediated by cytosol localized AGO2, then why cytosol AGO2 failed to influence cardiac performance while miR-320 showed a very strong effect. We reasoned that miR-320 was unlikely the only downstream target of cytosol AGO2 and conversely, miR-320 was also regulated by other transcriptional and translational regulator such as SP1, HIF-1α, histone deacetylase[46-48]. Therefore, the effects of miR-320 were not necessarily equal to cytosol AGO2 overexpression even when cytosol AGO2 was one of the direct regulators of miR-320. To further address this issue, we performed several experiments, finding that 1) miR-320 was upregulated by cytosol AGO2 but not nuclear AGO2 (Fig. S14A), 2) miR-320 was unable to regulate the expression of ANKRD1 in cardiomyocytes and vice versa (Fig. S14B-D), 3) Moreover, nuclear AGO2 aggravated ISO induced cardiomyocytes hypertrophy, which was not rescued by miR-320 knockdown (Fig. S14E and S14F). Therefore, miR-320 and ANKRD1 were two independent pathways mediated by different subcellular localized AGO2 (Fig. S14G).

The double face of ANKRD1 in nucleus and cytoplasm

Cytosolic ANKRD1 is present in the I-band region of the sarcomere as a member of the titin-N2A mechanosensory unit[26]. ANKRD1 mutations are directly linked to dilated cardiomyopathy as a result of disruption of the normal cardiac stretch-based signaling[25]. ANKRD1 carries the nuclear localization signal KKRKK, which enables its nuclear import[49]. In response to mechanical stretch, ANKRD1 acts as a transcription co-inhibitor and represses the expression of sarcomeric proteins[49]. ANKRD1 is upregulated in cardiac hypertrophy and heart failure[50,51], overexpression of ANKRD1 by recombinant adenovirus in engineered heart tissue causes contractile dysfunction[52]. However, ANKRD1 knockout and overexpression models have failed to clearly indicate the role of ANKRD1 in vivo[53]. One transgenic model showed an anti-

hypertrophy effect[54], whereas another study utilizing viral vector indicated that ANKRD1 overexpression could exacerbate pathologic remodeling in response to pressure overload[55]. ANKRD1 knockout mice fail to show phenotypic changes even under hemodynamic pressure load condition.[56,57] Our study provides a possible explanation for the contradiction between these studies by showing that cytosolic ANKRD1 protects against while nuclear ANKRD1 deteriorates pressure overload-induced cardiac remodeling. Mechanistically, instead of repressing cardiac troponin T and myosin light chain 2 in cultured cardiomyocytes[49,58], our in vivo data (RNA-seq and ChIP-PCR) and in vitro luciferase reporter assay conceivably suggest the direct transcriptional activation effect on MYH7 by nuclear ANKRD1. Though MYH6 remains unchanged, nuclear ANKRD1 overexpression increases MYH7/MYH6 ratio. However, further studies are required to reveal the detailed mechanisms underlying ANKRD1 mediated chromatin remodeling.

Moreover, ANKRD1 may be a generalized stress response in different cell types. We found that ANKRD1 was increased in endothelial cells but not cardiac fibroblasts under TGF-β1 stresses (Fig. S15A and S15B). Transmigration assay indicated that ANKRD1 knockdown decreased the migration of endothelial cells (Fig. S15C). However, EdU assay suggested that ANKRD1 had no effect on the proliferation of cardiac fibroblasts (Fig. S15D). Therefore, endothelial cells localized ANKRD1 might also participate in cardiovascular diseases, which are intriguing subjects for further study.

Comparison of therapeutic potential of the AGO2-ANKRD1-MYH7 axis

We report that shRNA targeting AGO2 or ANKRD1 delivered by rAAV9-tnt both protect against cardiac dysfunction in pressure overload-induced HF. Using rAAV to manipulate gene expression is becoming a promising therapy[59], especially since the

FDA approval of Luxturna® and Zolgensma®. Therefore, delivery of AGO2 or ANKRD1 shRNA by rAAV9 suggests a new therapeutic strategy against HF. In animal studies, we found that even with higher dosage, rAAV9 did not affect liver function of the mice (Fig. S16). However, it is intriguing to answer which percentage of cells would need to be targeted in human HF patients, assuming an AAV vector-based strategy would be applied. While it is difficult to accurately evaluate the percentage of cardiomyocytes needed to be targeted in HF patients, we can get some clue from animal studies. According to our study and other studies, a 50-70% of cardiomyocytes transduction was sufficient to induce alteration of cardiac performance[60-62]. Interestingly, we treated TAC-mice with different doses of rAAV9-tnt-shANKRD1, finding that the dosage with ~50-60% cardiomyocyte transfection improved cardiac function while a lower dosage with the transfection efficiency ~30% was unable to influence cardiac performance (Fig. S17). Therefore, it appeared that ~50-60**%** of cardiomyocytes should be targeted by using ANKRD1 inhibition as a therapeutic strategy to treat HF. However, this percentage might not apply to all rAAV9 delivered genes. For example, rAAV9 based overexpression of genes with secretory property which can freely translocate between cells might require a lower rAAV9 dosage to treat HF.

Alternatively, AGO2 or ANKRD1 knockdown by siRNA is another choice for clinical practice since siRNAs drugs are becoming a standard modality of pharmacotherapy, as exemplified by three approved siRNA drugs (patisiran, givosiran, and lumasiran)[63-65]. Comparatively, ANKRD1 seems to be more suitable to serve as a therapeutic target for HF, because ANKRD1 is specifically expressed in cardiomyocytes while AGO2 is wildly expressed in different tissues.

In terms of the in vivo effects of ANKRD1 knockdown, our study demonstrates

that shRNA mediated ANKRD1 knockdown improves cardiac performance in pressure-overloaded mice, which seems to be inconsistent with previous study showing no phenotype in pressure-overloaded ANKRD1 knockout mice[56,57]. We reasoned that shRNA-mediated ANKRD1 knockdown by rAAV9 is only able to partially decrease the upregulation of ANKRD1, whereas the physiological function of ANKRD1 in cytoplasm is largely reserved. As such, the protective effects by ANKRD1 shRNA are likely derived from reduced nuclear ANKRD1. In contrast, ANKRD1 knockout mice lost both its physiological function from cytosolic ANKRD1 as well as its pathological function of nuclear ANKRD1, which might explain the different between ANKRD1 knockout and knockdown. Therefore, the dosage and efficiency of shRNA or siRNAs must be carefully evaluated in clinical practise. Similarly, targeting MYH7 by siRNA also raises concerns about the dose-response effects, because MYH7 overexpression promotes cardiac hypertrophy and cardiac remodeling whereas Myh7 knockout by CRISPR/Cas9 causes impaired cardiovascular development due to sarcomere derangement[66].

Considering of the double face of ANKRD1 in cytoplasm and nucleus, it promotes us to test whether blockage of ANKRD1 nuclear import can protect against HF. The importin α/β mediates nuclear import of proteins containing the classical NLS including that identified in ANKRD1[67]. By using ivermectin, a potential inhibitor of importin α/β-mediated nuclear transport, nuclear ANKRD1 translocation is suppressed and cardiac dysfunction was remarkably improved.

Ivermectin is not a new drug but a WHO “Essential Medicine” already used in several different indications such as parasites infection[68]. Given the evidence of efficacy, safety, low cost, ivermectin is likely to have an impact on health and economic outcomes of HF, which needs to be further confirmed by randomized controlled trials

(RCT). Considering ivermectin is, after all, a broad-spectrum inhibitor of importin α/β-mediated nuclear transport, there might be some off-target effects mediated by other nuclear localized proteins, we constructed a ANKRD1 NLS mimetic peptide to specifically inhibit ANKRD1 nuclear import. However, strategies to improve the stability and delivery efficiency of ANPep peptide need future investigations.

Materials and Methods

Cell culture and transfection

Human myocardial cell line AC16 was from American Type Culture Collection (ATCC) and cultured in DMEM (Gibco, Grand Island, NY, USA) medium supplemented with 10% fetal bovine serum (FBS, Gibco). Murine cardiac muscle cell line HL-1, which was a kind gift from Professor Claycomb, was maintained in Claycomb medium (Sigma-Aldrich, St. Louis, MO, USA) with 10% FBS, supplemented with 100 μM norepinephrine and 4 mM L-glutamine. Neonatal rat ventricular myocytes (NRVMs) were separated from 1- to 3-day-old Sprague Dawley rats and cultured in DMEM medium containing 10% FBS, BrdU (0.1 mM), and penicillin/streptomycin, as described previously[20,69]. All cells were cultured at 37 °C in a humidified incubator with 5% CO_2.

Specific siRNAs, antisense oligonucleotides (ASOs), microRNA inhibitors were designed and synthesized by RiboBio (Guangzhou, China). Lipofectamine 2000 (Life Technologies, Carlsbad, CA, USA) was used to transfect these nucleic acids into cells according to the manufacturer's instructions. Adenoviruses were produced by Hanbio Biotechnology Co., Ltd. (Shanghai, China) to overexpress FLAG-tagged coding sequence of mouse *Ago2* and attached nuclear localization signal (NLS; sequence PKKKRKV) or nuclear export signal (NES; sequence LALKLAGLDIGS) in NRVMs and cell lines.

Animals

All animal experiments were approved by the Animal Care and Use Committee of Tongji Medical College, Huazhong University of Science and Technology (Wuhan, China). Male C57BL/6 mice used in this research were purchased from

GemPharmatech Co., Ltd. (Nanjing, China) and maintained under a 12h light/12h dark cycle at constant temperature (22 °C).

Transverse aortic constriction (TAC) surgery was performed to induce HF as described previously[20]. In brief, 8-week-old mice were anesthetized with 2% isoflurane and fixed in a supine position. A sternal median incision was made to expose aortic arch. Aortic arch and attached 27G needle were banded by a 7-0 silk. Then, the needle was removed to provide a lumen, and the chest was closed by 4-0 silk suture. Sham-operated mice underwent similar surgical procedures without aortic ligation.

One week after the surgery, the mice received 5×10^{11} vector genome (vg) of the recombinant adeno-associated virus serotype 9 (rAAV9) (ViGene Biosciences, Shandong, China) via tail vein injection to manipulate gene expression. In addition, the mice were intragastrically administrated with ivermectin (1 mg/kg) or DMSO every other day. The cardiac function was evaluated via echocardiography (Vevo1100, VisualSonics, Toronto, Canada) and Millar catheter system (Millar Instruments, Houston, Texas, USA) eight weeks after TAC surgery, as described previously[20].

ANPep peptide (YGRKKRRQRRREDLEIIVQLKKRKKYKKTK) was synthesized with 98% purity by Sangon Biotech Co., Ltd (Shanghai, China). Two weeks after the TAC surgery, the mice were intraperitoneally injected with ANPep (25 mg/kg) or PBS every day for four weeks. The cardiac function was evaluated six weeks after TAC surgery. Strategies for all animal experiments were summarized in Figure S18.

Cell fraction isolation

Nuclear and cytosolic fractions were separated using NE-PER Nuclear and Cytoplasmic Extraction Reagents (#78833, Thermo Fisher Scientific, MA, USA), according to the manufacturer's recommended protocols.

521

522 **Western blotting**

523 Western blotting was performed as previously described[10]. The protein lysates
524 were separated in sodium dodecyl sulfate polyacrylamide gel electrophoresis (SDS-
525 PAGE) and transferred onto polyvinylidene fluoride (PVDF) membranes. After 1h
526 blocking with 5% BSA at room temperature, the membranes were incubated with
527 primary antibodies overnight at 4 °C. Horseradish peroxidase (HRP)-conjugated
528 secondary antibodies and ECL detection regents (Beyotime, Shanghai, China) were
529 used to detect protein signals. The primary antibodies used in this study are listed as
530 follows: AGO2 (#ab156870, abcam), ANKRD1 (#A6192, Abclonal), C3 (#21337-1-AP,
531 Proteintech), MYH7 (#A7564, Abclonal), MYH6 (#22281-1-AP, Proteintech), CES1
532 (#PA5-47802, Thermo Fisher Scientific), FLAG (#AE005, Abclonal), Lamin B1
533 (#12987-1-AP, Proteintech), GAPDH (#60004-1-lg, Proteintech). The full unedited gel
534 data was shown in Figure S19.

535

536 **Quantitative reverse transcription PCR (RT-qPCR)**

537 Total RNA was extracted from heart tissue and cells using TRIzol regent
538 (Invitrogen, Carlsbad, CA, USA) and reverse-transcribed into cDNA using HiScript II
539 Q Select RT SuperMix for qPCR (+gDNA wiper) Kit (Vazyme Biotech Co., Ltd, China).
540 Real-time PCR was performed using SYBR Green Mix (KAPA Biosystems,
541 Wilmington, MA, USA) on a 7900HT FAST real-time PCR system (Life Technologies).
542 GAPDH expression was used as a normalization control. All primer sequences were
543 listed in Table S1.

544

545 **RNA sequencing**

RNA sequencing and data analysis were performed by Seqhealth Technology Co., LTD (Wuhan, China). Total RNA from heart tissue and cells was extracted using TRIzol, and then reverse-transcribed according to standard procedures. The libraries were submitted to the Novaseq 6000 platform for high-throughput sequencing. Differentially expressed genes (DEGs) were analyzed using the edgeR software package. Sequencing raw data were deposited in the NCBI Sequence Read Archive (SRA) database (PRJNA1083053 and PRJNA1083207).

Chromatin immunoprecipitation (ChIP)-PCR/sequencing

ChIP assay was performed described previously[10]. In brief, minced hearts or cells were fixed with 1% formaldehyde for 10 min at room temperature, and then quenched with glycine at a final concentration of 125 mM. The fixed samples were homogenized in lysis buffer and sonicated to shear DNA to the length of 200-1000 bps, which were then incubated with anti-AGO2 antibody (#H00027161-M01, Abnova), anti-FLAG antibody (#AE005, Abclonal) or normal control IgG (#AC011, Abclonal) at 4 °C overnight. Antibody-chromatin complexes were enriched with protein A/G magnetic beads (#88802, Thermo Fisher Scientific). Next, immunoprecipitated DNA was cross-link reversed and purified with QIAquick PCR Purification Kit (Qiagen). Enrichment at the promoter of target genes was detected by real-time PCR and sequencing. The primer sequences were listed in Table S1. The sequencing and subsequent analysis were conducted by Personal Biotechnology Co. Ltd. (Shanghai, China) according to standard procedures.

CUT&Tag assay

CUT&Tag assay was performed with Hyperactive Universal CUT&Tag Assay Kit

for Illumina Pro kit (Vazyme, TD903) according to the manufacturer's recommended protocol. Firstly, approximately 1×10^4 cells were collected into EP tubes by centrifugation and washed with 100 μl Wash Buffer. Then, 10 μl Binding Buffer washed ConA beads were added followed by incubation at room temperature for 5-10 minutes. Secondly, after removing the supernatant, resuspend the cells using 50 μl Antibody Buffer followed by adding 1 μg anti-FLAG antibody (#AE005, Abclonal) and incubating overnight at 4 °C. Thirdly, discarded the supernatant and added 50 μl corresponding secondary antibody (diluted with Dig-wash Buffer at a ratio of 1:100) followed by incubation at room temperature for 1 h. Then, removed the supernatant and washed three times with 800 μl Dig-wash Buffer. Next, 100 μl Hyperactive pG-Tn5/pA-Tn5 (0.04 μM) was added to each sample and incubated at room temperature for 1 h, followed by three times washing with 800 μl Dig-300 buffer. Lastly, after discarding the supernatant of the specimen, 300 μl Tagmentation Buffer was added followed by 1h incubation at 37 °C. Finally, DNA was extracted and PCR was performed to amplify the libraries. The libraries were sequenced by Novogene Biotechnology Co. Ltd. (Tianjin, China).

RNA immunoprecipitation (RIP)

Ultra-violet-irradiated cells were harvested with lysis buffer, and the lysates were incubated with anti-FLAG antibody (#AE005, Abclonal) or IgG (#AC011, Abclonal) at 4 °C overnight. Then, protein A/G magnetic beads (Thermo Fisher Scientific) were added to capture protein-RNA complex. RNA from the complex was extracted by TRIzol regent and reverse-transcribed into first-strand cDNA with strand-specific primer for real-time PCR analysis. All primers were listed in Table S1.

Dual-luciferase reporter assay

The promoter region (-2000 to +500) of corresponding genes was cloned into pGL3-Basic luciferase reporter vector (Promega). HEK293T cells were co-transfected with luciferase reporter vector, *Renilla* luciferase reporter plasmid, and experimental vectors. After 48 h, luciferase activity was detected by Dual-Luciferase Reporter Assay System (Promega) according to the manufacturer's instructions. *Renilla* luciferase activity served as a control for normalization.

Immunofluorescence (IF)

Briefly, the cells were fixed with 4% paraformaldehyde, followed by permeabilization with 0.5% Triton-100. After blocking with 5% BSA for 45 min at room temperature, the cells were incubated with indicated primary antibodies (anti-AGO2, #MAB19576, Abnova; anti-α-actinin, #A7811, Sigma-Aldrich; anti-FLAG, #AE005, Abclonal; anti-GFP, #50430-2-AP, Proteintech; anti-TNI, #66376-1-lg, Proteintech; anti-Vimentin, #GB12192, Servicebio; anti-CD31, #GB12063, Servicebio) at 4 °C overnight. Finally, the cells were incubated with fluorophore-conjugated secondary antibodies and Hoechst for 45 min at room temperature. Images were taken using Zeiss Axio Imager A2 microscope and NIKON Eclipse T confocal microscope.

Histology and morphometric analysis

Mice heart tissues were fixed with 4% paraformaldehyde, then embedded in paraffin, and cut into 4 μm sections. The sections were stained with hematoxylin–eosin (HE) and Sirius Red to evaluate the cardiac morphology and fibrosis. The images were analyzed and quantified by Image J software.

Human samples

Human failing heart tissue were collected from patients diagnosed as dilated cardiomyopathy during heart transplantation, and the normal hearts were collected from donors who died in traffic accidents, which were approved by the Clinical Research Committee of Tongji Medical College (Wuhan, China). The clinical characteristics of normal donors and patients were listed in Table S2.

Rapid amplification of cDNA ends (RACE)

The 5' and 3' RACE were performed according to the standard protocol[70,71]. For 5' RACE, RNA extracted from mouse heart was reverse-transcribed into first-strand cDNA with Ankrd1-GSP-RT primer. Then, a poly(A) tail was attached to the first-strand cDNA. Next, first round amplification was conducted using Q_T, Q_O, and Ankrd1-GSP1 primers, and a second-round amplification is carried out using Q_I and Ankrd1-GSP2 primers to quench the non-specific amplifications. For 3' RACE, the Q_T primer was used for reverse-transcription. The first round was amplified using Q_O, and Ankrd1-GSP3 primers, and Q_I and Ankrd1-GSP4 primers were used for second set of amplification. Agarose gel electrophoresis and sequencing were performed to analyze the final amplification products. All primers were listed in Table S1. The sequences of Ankrd1 PATs were presented in Table S3.

Statistical analysis

Data are presented as mean ± SEM, and statistical analyses were performed using GraphPad Prism (v8.0) (San Diego, CA, USA). Differences between 2 groups were compared student's t-test. One-way ANOVA with Tukey test was used to analyze the statistical differences in multiple comparisons. Statistical significance was set at $P <$

646 0.05.

Data Availability Statement

The authors confirm that the data supporting the findings of this study are available within the article or its supplemental materials.

Acknowledgements

We thank professor Xiang-Dong Fu and our colleagues in Dr. Wang's group for technical assistance and stimulating discussions during the course of this investigation. This work was supported by grants from the National Natural Science Foundation of China (nos. U22A20266, 82170273, 82100400, 82241034, 82270363), Program for HUST Academic Frontier Youth Team 2019QYTD08, Knowledge Innovation Program of Wuhan-Shuguang Project 2022020801020451 and Tongji Hospital Science Fund for outstanding Young Scholars (No. 2020YBKY022). The funders had no role in study design, data collection and analysis, manuscript preparation, or decision to publish.

Author Contributions

R.X. designed the study, analyzed and interpreted the data, and drafted the paper; S.Y., G.H., J.Z., K.J., Y.T., J.F., Y.Z., and F.W. participated in acquiring the data; H.L., C.C., and D.W.W. designed the work and drafted the paper.

Declaration of Interests

The authors declare no competing interests.

Keywords: heart failure; nuclear AGO2; non-coding RNA; transcriptional regulation; MYH7/MYH6 ratio

671 ## References

672 1. Yancy, C.W., Jessup, M., Bozkurt, B., Butler, J., Casey, D.E., Colvin, M.M., Drazner, M.H.,
673 Filippatos, G.S., Fonarow, G.C., Givertz, M.M., et al. (2017). 2017 ACC/AHA/HFSA Focused
674 Update of the 2013 ACCF/AHA Guideline for the Management of Heart Failure: A Report of the
675 American College of Cardiology/American Heart Association Task Force on Clinical Practice
676 Guidelines and the Heart Failure Society of America. J. Am. Coll. Cardiol. *70*, 776-803.
677 2. Zannad, F. (2018). Rising incidence of heart failure demands action. The Lancet *391*, 518-519.
678 3. Vaduganathan, M., Claggett, B.L., Jhund, P.S., Cunningham, J.W., Pedro Ferreira, J., Zannad, F.,
679 Packer, M., Fonarow, G.C., McMurray, J.J.V., and Solomon, S.D. (2020). Estimating lifetime
680 benefits of comprehensive disease-modifying pharmacological therapies in patients with heart
681 failure with reduced ejection fraction: a comparative analysis of three randomised controlled
682 trials. The Lancet *396*, 121-128.
683 4. Tham, Y.K., Bernardo, B.C., Ooi, J.Y.Y., Weeks, K.L., and McMullen, J.R. (2015). Pathophysiology
684 of cardiac hypertrophy and heart failure: signaling pathways and novel therapeutic targets.
685 Arch. Toxicol. *89*, 1401-1438.
686 5. Hang, C.T., Yang, J., Han, P., Cheng, H.-L., Shang, C., Ashley, E., Zhou, B., and Chang, C.-P. (2010).
687 Chromatin regulation by Brg1 underlies heart muscle development and disease. Nature *466*,
688 62-67.
689 6. Holubarsch, C., Goulette, R.P., Litten, R.Z., Martin, B.J., Mulieri, L.A., and Alpert, N.R. (1985).
690 The economy of isometric force development, myosin isoenzyme pattern and myofibrillar
691 ATPase activity in normal and hypothyroid rat myocardium. Circulation Research *56*, 78-86.
692 7. Sugiura, S., Kobayakawa, N., Fujita, H., Yamashita, H., Momomura, S.-i., Chaen, S., Omata, M.,
693 and Sugi, H. (1998). Comparison of Unitary Displacements and Forces Between 2 Cardiac
694 Myosin Isoforms by the Optical Trap Technique. Circulation Research *82*, 1029-1034.
695 8. Krenz, M., and Robbins, J. (2004). Impact of beta-myosin heavy chain expression on cardiac
696 function during stress. J. Am. Coll. Cardiol. *44*, 2390-2397.
697 9. Han, P., Li, W., Lin, C.-H., Yang, J., Shang, C., Nurnberg, S.T., Jin, K.K., Xu, W., Lin, C.-Y., Lin, C.-J.,
698 et al. (2014). A long noncoding RNA protects the heart from pathological hypertrophy. Nature
699 *514*, 102-106.
700 10. Li, H., Fan, J., Zhao, Y., Zhang, X., Dai, B., Zhan, J., Yin, Z., Nie, X., Fu, X.-D., Chen, C., et al. (2019).
701 Nuclear miR-320 Mediates Diabetes-Induced Cardiac Dysfunction by Activating Transcription
702 of Fatty Acid Metabolic Genes to Cause Lipotoxicity in the Heart. Circulation Research *125*,
703 1106-1120.
704 11. Li, H., Zhang, X., Wang, F., Zhou, L., Yin, Z., Fan, J., Nie, X., Wang, P., Fu, X.-D., Chen, C., et al.
705 (2016). MicroRNA-21 Lowers Blood Pressure in Spontaneous Hypertensive Rats by
706 Upregulating Mitochondrial Translation. Circulation *134*, 734-751.
707 12. Zhang, X., Zuo, X., Yang, B., Li, Z., Xue, Y., Zhou, Y., Huang, J., Zhao, X., Zhou, J., Yan, Y., et al.
708 (2014). MicroRNA Directly Enhances Mitochondrial Translation during Muscle Differentiation.
709 Cell *158*, 607-619.
710 13. Trabucchi, M., and Mategot, R. (2019). Subcellular Heterogeneity of the microRNA Machinery.
711 Trends Genet. *35*, 15-28.
712 14. Zhang, G.-Q., Wang, S.-Q., Chen, Y., Fu, L.-Y., Xu, Y.-N., Li, L., Tao, L., and Shen, X.-C. (2021).
713 MicroRNAs Regulating Mitochondrial Function in Cardiac Diseases. Front. Pharmacol. *12*.
714 15. Bajpai, P., Koc, E., Sonpavde, G., Singh, R., and Singh, K.K. (2019). Mitochondrial localization,

import, and mitochondrial function of the androgen receptor. J. Biol. Chem. *294*, 6621-6634.

16. Lu, J., Wu, T., Zhang, B., Liu, S., Song, W., Qiao, J., and Ruan, H. (2021). Types of nuclear localization signals and mechanisms of protein import into the nucleus. Cell Communication and Signaling *19*, 60.
17. Bandiera, S., Rüberg, S., Girard, M., Cagnard, N., Hanein, S., Chrétien, D., Munnich, A., Lyonnet, S., and Henrion-Caude, A. (2011). Nuclear outsourcing of RNA interference components to human mitochondria. PLoS One *6*, e20746.
18. Benhamed, M., Herbig, U., Ye, T., Dejean, A., and Bischof, O. (2012). Senescence is an endogenous trigger for microRNA-directed transcriptional gene silencing in human cells. Nat. Cell Biol. *14*, 266-275.
19. Weinmann, L., Höck, J., Ivacevic, T., Ohrt, T., Mütze, J., Schwille, P., Kremmer, E., Benes, V., Urlaub, H., and Meister, G. (2009). Importin 8 Is a Gene Silencing Factor that Targets Argonaute Proteins to Distinct mRNAs. Cell *136*, 496-507.
20. Zhang, X., Yuan, S., Li, H., Zhan, J., Wang, F., Fan, J., Nie, X., Wang, Y., Wen, Z., Chen, Y., et al. (2021). The double face of miR-320: cardiomyocytes-derived miR-320 deteriorated while fibroblasts-derived miR-320 protected against heart failure induced by transverse aortic constriction. Signal Transduction and Targeted Therapy *6*, 69.
21. Gladka, M.M., Molenaar, B., de Ruiter, H., van der Elst, S., Tsui, H., Versteeg, D., Lacraz, G.P.A., Huibers, M.M.H., van Oudenaarden, A., and van Rooij, E. (2018). Single-Cell Sequencing of the Healthy and Diseased Heart Reveals Cytoskeleton-Associated Protein 4 as a New Modulator of Fibroblasts Activation. Circulation *138*, 166-180.
22. Xiao, R., Chen, J.-Y., Liang, Z., Luo, D., Chen, G., Lu, Z.J., Chen, Y., Zhou, B., Li, H., Du, X., et al. (2019). Pervasive Chromatin-RNA Binding Protein Interactions Enable RNA-Based Regulation of Transcription. Cell *178*, 107-121.e118.
23. Tarallo, R., Giurato, G., Bruno, G., Ravo, M., Rizzo, F., Salvati, A., Ricciardi, L., Marchese, G., Cordella, A., Rocco, T., et al. (2017). The nuclear receptor ERβ engages AGO2 in regulation of gene transcription, RNA splicing and RISC loading. Genome Biol. *18*, 189.
24. Li, H., Zhan, J., Zhao, Y., Fan, J., Yuan, S., Yin, Z., Dai, B., Chen, C., and Wang, D.W. (2020). Identification of ncRNA-Mediated Functions of Nucleus-Localized miR-320 in Cardiomyocytes. Molecular Therapy - Nucleic Acids *19*, 132-143.
25. Moulik, M., Vatta, M., Witt, S.H., Arola, A.M., Murphy, R.T., McKenna, W.J., Boriek, A.M., Oka, K., Labeit, S., Bowles, N.E., et al. (2009). ANKRD1, the Gene Encoding Cardiac Ankyrin Repeat Protein, Is a Novel Dilated Cardiomyopathy Gene. J. Am. Coll. Cardiol. *54*, 325-333.
26. Miller, M.K., Bang, M.-L., Witt, C.C., Labeit, D., Trombitas, C., Watanabe, K., Granzier, H., McElhinny, A.S., Gregorio, C.C., and Labeit, S. (2003). The Muscle Ankyrin Repeat Proteins: CARP, ankrd2/Arpp and DARP as a Family of Titin Filament-based Stress Response Molecules. J. Mol. Biol. *333*, 951-964.
27. Swynghedauw, B. (1986). Developmental and functional adaptation of contractile proteins in cardiac and skeletal muscles. Physiol. Rev. *66*, 710-771.
28. Miyata, S., Minobe, W., Bristow, M.R., and Leinwand, L.A. (2000). Myosin Heavy Chain Isoform Expression in the Failing and Nonfailing Human Heart. Circulation Research *86*, 386-390.
29. Abraham, W.T., Gilbert, E.M., Lowes, B.D., Minobe, W.A., Larrabee, P., Roden, R.L., Dutcher, D., Sederberg, J., Lindenfeld, J.A., Wolfel, E.E., et al. (2002). Coordinate changes in Myosin heavy chain isoform gene expression are selectively associated with alterations in dilated

cardiomyopathy phenotype. Mol. Med. *8*, 750-760.

30. Yue, P., Xia, S., Wu, G., Liu, L., Zhou, K., Liao, H., Li, J., Zheng, X., Guo, Y., Hua, Y., et al. (2021). Attenuation of Cardiomyocyte Hypertrophy via Depletion Myh7 using CASAAV. Cardiovasc. Toxicol. *21*, 255-264.

31. Kosyna, F.K., and Depping, R. (2018). Controlling the Gatekeeper: Therapeutic Targeting of Nuclear Transport. Cells.

32. Wagstaff, K.M., Rawlinson, S.M., Hearps, A.C., and Jans, D.A. (2011). An AlphaScreen®-Based Assay for High-Throughput Screening for Specific Inhibitors of Nuclear Import. Journal of Biomolecular Screening *16*, 192-200.

33. Ravid, R., Siany, A., Rivkin, N., Eitan, C., Marmor-Kollet, H., Yanowski, E., Savidor, A., Levin, Y., Rot, G., Meister, G., et al. (2020). A nuclear role for ARGONAUTE-2 in regulation of neuronal alternative polyadenylation. bioRxiv, 2020.2012.2015.422806.

34. Gagnon, Keith T., Li, L., Chu, Y., Janowski, Bethany A., and Corey, David R. (2014). RNAi Factors Are Present and Active in Human Cell Nuclei. Cell Reports *6*, 211-221.

35. Sharma, N.R., Wang, X., Majerciak, V., Ajiro, M., Kruhlak, M., Meyers, C., and Zheng, Z.-M. (2016). Cell Type- and Tissue Context-dependent Nuclear Distribution of Human Ago2. J. Biol. Chem. *291*, 2302-2309.

36. Patil, A., Nakai, K., and Nakamura, H. (2011). HitPredict: a database of quality assessed protein–protein interactions in nine species. Nucleic Acids Res. *39*, D744-D749.

37. Lin, J.-r., and Hu, J. (2013). SeqNLS: nuclear localization signal prediction based on frequent pattern mining and linear motif scoring. PLoS One *8*, e76864.

38. Carissimi, C., Laudadio, I., Cipolletta, E., Gioiosa, S., Mihailovich, M., Bonaldi, T., Macino, G., and Fulci, V. (2015). ARGONAUTE2 cooperates with SWI/SNF complex to determine nucleosome occupancy at human Transcription Start Sites. Nucleic Acids Res. *43*, 1498-1512.

39. Kim, D.H., Sætrom, P., Snøve, O., and Rossi, J.J. (2008). MicroRNA-directed transcriptional gene silencing in mammalian cells. Proceedings of the National Academy of Sciences *105*, 16230-16235.

40. Portnoy, V., Lin, S.H.S., Li, K.H., Burlingame, A., Hu, Z.-H., Li, H., and Li, L.-C. (2016). saRNA-guided Ago2 targets the RITA complex to promoters to stimulate transcription. Cell Res. *26*, 320-335.

41. Taliaferro, J.M., Aspden, J.L., Bradley, T., Marwha, D., Blanchette, M., and Rio, D.C.R. (2013). Two new and distinct roles for Drosophila Argonaute-2 in the nucleus: alternative pre-mRNA splicing and transcriptional repression. Genes Dev. *27*, 378-389.

42. Jaehning, J.A. (2010). The Paf1 complex: Platform or player in RNA polymerase II transcription? Biochimica et Biophysica Acta (BBA) - Gene Regulatory Mechanisms *1799*, 379-388.

43. Weintraub, A.S., Li, C.H., Zamudio, A.V., Sigova, A.A., Hannett, N.M., Day, D.S., Abraham, B.J., Cohen, M.A., Nabet, B., Buckley, D.L., et al. (2017). YY1 Is a Structural Regulator of Enhancer-Promoter Loops. Cell *171*, 1573-1588.e1528.

44. Elbarbary, R.A., Miyoshi, K., Myers, J.R., Du, P., Ashton, J.M., Tian, B., and Maquat, L.E. (2017). Tudor-SN–mediated endonucleolytic decay of human cell microRNAs promotes G1/S phase transition. Science *356*, 859-862.

45. Yu, S., and Kim, V.N. (2020). A tale of non-canonical tails: gene regulation by post-transcriptional RNA tailing. Nature Reviews Molecular Cell Biology *21*, 542-556.

46. Sato, S., Katsushima, K., Shinjo, K., Hatanaka, A., Ohka, F., Suzuki, S., Naiki-Ito, A., Soga, N.,

Takahashi, S., and Kondo, Y. (2016). Histone Deacetylase Inhibition in Prostate Cancer Triggers miR-320–Mediated Suppression of the Androgen Receptor. Cancer Res. *76*, 4192-4204.

47. Wu, Y.-Y., Chen, Y.-L., Jao, Y.-C., Hsieh, I.S., Chang, K.-C., and Hong, T.-M. (2014). miR-320 regulates tumor angiogenesis driven by vascular endothelial cells in oral cancer by silencing neuropilin 1. Angiogenesis *17*, 247-260.
48. Zhan, J., Jin, K., Ding, N., Zhou, Y., Hu, G., Yuan, S., Xie, R., Wen, Z., Chen, C., Li, H., et al. (2023). Positive feedback loop of miR-320 and CD36 regulates the hyperglycemic memory-induced diabetic diastolic cardiac dysfunction. Molecular Therapy - Nucleic Acids *31*, 122-138.
49. Jeyaseelan, R., Poizat, C., Baker, R.K., Abdishoo, S., Isterabadi, L.B., Lyons, G.E., and Kedes, L. (1997). A Novel Cardiac-Restricted Target for Doxorubicin: CARP, A NUCLEAR MODULATOR OF GENE EXPRESSION IN CARDIAC PROGENITOR CELLS AND CARDIOMYOCYTES*. J. Biol. Chem. *272*, 22800-22808.
50. Aihara, Y., Kurabayashi, M., Saito, Y., Ohyama, Y., Tanaka, T., Takeda, S.-i., Tomaru, K., Sekiguchi, K.-i., Arai, M., Nakamura, T., et al. (2000). Cardiac Ankyrin Repeat Protein Is a Novel Marker of Cardiac Hypertrophy. Hypertension *36*, 48-53.
51. Torrado, M., López, E., Centeno, A., Castro-Beiras, A., and Mikhailov, A.T. (2004). Left–right asymmetric ventricular expression of CARP in the piglet heart: regional response to experimental heart failure. Eur. J. Heart Fail. *6*, 161-172.
52. Zolk, O., Marx, M., Jäckel, E., El-Armouche, A., and Eschenhagen, T. (2003). β-Adrenergic stimulation induces cardiac ankyrin repeat protein expression: involvement of protein kinase A and calmodulin-dependent kinase. Cardiovasc. Res. *59*, 563-572.
53. Murphy, N.P., Lubbers, E.R., and Mohler, P.J. (2020). Advancing our understanding of ANKRD1 in cardiac development and disease. Cardiovasc. Res. *116*, 1402-1404.
54. Song, Y., Xu, J., Li, Y., Jia, C., Ma, X., Zhang, L., Xie, X., Zhang, Y., Gao, X., Zhang, Y., et al. (2012). Cardiac ankyrin repeat protein attenuates cardiac hypertrophy by inhibition of ERK1/2 and TGF-β signaling pathways. PLoS One *7*, e50436.
55. Chen, C., Shen, L., Cao, S., Li, X., Xuan, W., Zhang, J., Huang, X., Bin, J., Xu, D., Li, G., et al. (2014). Cytosolic CARP promotes angiotensin II- or pressure overload-induced cardiomyocyte hypertrophy through calcineurin accumulation. PLoS One *9*, e104040.
56. Bang, M.-L., Gu, Y., Dalton, N.D., Peterson, K.L., Chien, K.R., and Chen, J. (2014). The muscle ankyrin repeat proteins CARP, Ankrd2, and DARP are not essential for normal cardiac development and function at basal conditions and in response to pressure overload. PLoS One *9*, e93638.
57. Zhong, L., Chiusa, M., Cadar, A.G., Lin, A., Samaras, S., Davidson, J.M., and Lim, C.C. (2015). Targeted inhibition of ANKRD1 disrupts sarcomeric ERK-GATA4 signal transduction and abrogates phenylephrine-induced cardiomyocyte hypertrophy. Cardiovasc. Res. *106*, 261-271.
58. Zou, Y., Evans, S., Chen, J., Kuo, H.C., Harvey, R.P., and Chien, K.R. (1997). CARP, a cardiac ankyrin repeat protein, is downstream in the Nkx2-5 homeobox gene pathway. Development *124*, 793-804.
59. Emmanuel Shanan, N., Smith, J.K., Hsi, J., Tseng, Y.-S., Kaplan, M., Mietzsch, M., Chipman, P., Asokan, A., McKenna, R., and Agbandje-McKenna, M. (2022). Structurally Mapping Antigenic Epitopes of Adeno-associated Virus 9: Development of Antibody Escape Variants. J. Virol. *96*, e01251-01221.
60. Bruegmann, T., Boyle, P.M., Vogt, C.C., Karathanos, T.V., Arevalo, H.J., Fleischmann, B.K.,

Trayanova, N.A., and Sasse, P. (2016). Optogenetic defibrillation terminates ventricular arrhythmia in mouse hearts and human simulations. The Journal of Clinical Investigation *126*, 3894-3904.

61. Vogt, C.C., Bruegmann, T., Malan, D., Ottersbach, A., Roell, W., Fleischmann, B.K., and Sasse, P. (2015). Systemic gene transfer enables optogenetic pacing of mouse hearts. Cardiovasc. Res. *106*, 338-343.

62. Werfel, S., Jungmann, A., Lehmann, L., Ksienzyk, J., Bekeredjian, R., Kaya, Z., Leuchs, B., Nordheim, A., Backs, J., Engelhardt, S., et al. (2014). Rapid and highly efficient inducible cardiac gene knockout in adult mice using AAV-mediated expression of Cre recombinase. Cardiovasc. Res. *104*, 15-23.

63. Hoy, S.M. (2018). Patisiran: First Global Approval. Drugs *78*, 1625-1631.

64. Scott, L.J. (2020). Givosiran: First Approval. Drugs *80*, 335-339.

65. Scott, L.J., and Keam, S.J. (2021). Lumasiran: First Approval. Drugs *81*, 277-282.

66. Hesaraki, M., Bora, U., Pahlavan, S., Salehi, N., Mousavi, S.A., Barekat, M., Rasouli, S.J., Baharvand, H., Ozhan, G., and Totonchi, M. (2022). A Novel Missense Variant in Actin Binding Domain of MYH7 Is Associated With Left Ventricular Noncompaction. Frontiers in Cardiovascular Medicine *9*.

67. Kosugi, S., Hasebe, M., Matsumura, N., Takashima, H., Miyamoto-Sato, E., Tomita, M., and Yanagawa, H. (2009). Six Classes of Nuclear Localization Signals Specific to Different Binding Grooves of Importin α. J. Biol. Chem. *284*, 478-485.

68. Ashour, D.S. (2019). Ivermectin: From theory to clinical application. Int. J. Antimicrob. Agents *54*, 134-142.

69. Ravi, V., Jain, A., Taneja, A., Chatterjee, K., and Sundaresan, N.R. (2021). Isolation and Culture of Neonatal Murine Primary Cardiomyocytes. Current Protocols *1*, e196.

70. Scotto‐Lavino, E., Du, G., and Frohman, M.A. (2006). 5′ end cDNA amplification using classic RACE. Nat. Protoc. *1*, 2555-2562.

71. Scotto‐Lavino, E., Du, G., and Frohman, M.A. (2006). 3′ End cDNA amplification using classic RACE. Nat. Protoc. *1*, 2742-2745.

List of Figure Captions

Figure 1. Upregulation of AGO2 in cardiomyocytes of failing hearts.

(A) and (B) Western blotting analysis of AGO2 in cytoplasm and nucleus of hearts of Sham and TAC-induced HF mice (n = 6). (C) Co-localization analysis of AGO2 with cardiomyocyte-specific marker. (D) and (E) Western blotting analysis of AGO2 in cytoplasm and nucleus of human hearts (n = 4). Student's t-test was used in (B) and (E).

Figure 2. Elevated nuclear AGO2 impairs cardiac performance in TAC-operated mice.

(A) Western blotting analysis of AGO2 in mice hearts (n = 6). Echocardiographic analysis (B) (n = 8-9) and Hemodynamic parameters (C) (n = 6-7) of mice under AGO2 inhibition. (D) Representative images of HE (n = 8-9) and Sirius Red (n = 8-9) staining. (E) Quantitative analysis of cell surface and fibrosis area. Echocardiographic analysis (F) (n = 8-10) and Hemodynamic parameters (G) (n = 7-8) of mice with cytosolic or nuclear AGO2 overexpression. (J) Western blotting analysis of FLAG-tagged AGO2 in cytoplasm and nucleus of hearts. (H) Representative images of HE and Sirius Red staining. (I) Quantitative analysis of cell surface and fibrosis area. One-way ANOVA with the Tukey post-test was used.

Figure 3. ANKRD1 as a direct target of nuclear AGO2 in TAC-treated mice.

(A) Strategy to identify the targets of nuclear AGO2. (B). AGO2 binding sites on *ANKRD1* and *C3* promoter identified by CUT&Tag in AC16 cells expressing FLAG-tagged nuclear AGO2. (C) ChIP analysis using anti-AGO2 for the promoter region of *Ankrd1* and *C3* in mice hearts (n = 4). (D) and (E) Western blotting analysis of ANKRD1 and C3 in rAAV-AGO2-NLS/NES-treated mice (n = 6). (F) and (G) Western

blotting analysis of ANKRD1 protein level in ad-AGO2-NLS/NES-treated NRVMs (n = 6). (H) and (I) Western blotting analysis of ANKRD1 protein level in AGO2 knockdown NRVMs (n = 6). One-way ANOVA with the Tukey post-test was used in (E) and (G). Student's t-test was used in (C) and (I).

Figure 4. Nuclear AGO2 acted as a transcriptional cofactor to enhance ANKRD1 transcription.

(A) and (B)Regulation of AGO2 on *ANKRD1* transcription detected by luciferase reporter assays in HEK293T cells (n = 6). (C) ChIP analysis using anti-AGO2 for the promoter region of *Ankrd1* in HL-1 cells with actinomycin D treatment for 4 h (n = 4). (D) Schematic illustration of *Ankrd1* PATs. (E) ChIP analysis using anti-FLAG for the promoter region of *Ankrd1* in FLAG-tagged AGO2-NLS-overexpressed HL-1 cells transfected with ASO specific to sense- or antisense PATs. (F) RIP assay to determine the interaction between sense- or antisense PATs and AGO2 using anti- FLAG or IgG (negative control) in FLAG-tagged AGO2-NLS-overexpressed HL-1 cells (n = 4). (G) Strategy to identify the crucial miRNAs mediating the interaction between AGO2 and sense PAT. (H) ChIP analysis using anti- FLAG for the promoter region of *Ankrd1* in FLAG-tagged AGO2-NLS-overexpressed HL-1 cells transfected with inhibitors targeting miR-92a-3p (n = 4). (I) RIP assay to determine the interaction between AGO2 and sense PAT using anti-FLAG in FLAG-tagged AGO2-NLS-overexpressed HL-1 cells transfected with inhibitor targeting miR-92a-3p (n = 4). (J) Schematic diagram of the working model of AGO2 in *ANKRD1* transcriptional regulation. One-way ANOVA with the Tukey post-test was used in (E). Student's t-test was used in (A), (B), (C), (F), (H) and (I).

Figure 5. Nuclear AGO2 exacerbated TAC-induced cardiac dysfunction via ANKRD1.

(A) Western blotting analysis of ANKRD1 in mice hearts. Echocardiographic analysis (B) and Hemodynamic parameters (C) of mice subjected to different treatments ($n = 6$). (D) Representative images of HE and Sirius Red staining ($n = 6$). (E) Quantitative analysis of cell surface and fibrosis area. (F) Western blotting analysis of ANKRD1 in cytoplasm and nucleus of rAAV-AGO2-NLS/NES-treated mice hearts. Echocardiographic analysis (G) and Hemodynamic parameters (H) of mice subjected to different treatments ($n = 6$). One-way ANOVA with the Tukey post-test was used.

Figure 6. Nuclear ANKRD1 induced pathological MYH7 expression in TAC-operated mice.

(A) Strategy to identify the targets of nuclear ANKRD1. (B) and (C) Western blotting analysis of MYH7, MYH6, and CES1 in rAAV-ANKRD1-NLS/NES-treated mice hearts ($n = 6$). (D) Regulation of ANKRD1 on MYH7 transcription detected by luciferase reporter assays in HEK293T cells ($n = 6$). (E) ChIP analysis using anti-FLAG for the promoter region of *Myh7* in rAAV-ANKRD1-NLS-treated mice hearts ($n = 4$). (F) ChIP-seq profiles using anti-FLAG for the promoter region of *Myh7* in rAAV-ANKRD1-NLS-treated mice hearts. (G) Schematic diagram of the working model of nuclear AGO2 in heart failure. One-way ANOVA with the Tukey post-test was used in (C). Student's t-test was used in (D) and (E).

Figure 7. Ivermectin suppressed ANKRD1 nucleus import and improved cardiac performance in TAC-operated mice.

Echocardiographic analysis (A) and Hemodynamic parameters (B) of mice treated with

ivermectin (n = 6). (C) and (D) Western blotting analysis of ANKRD1 in cytoplasm and nucleus of hearts (n = 6). (E) and (F) Western blotting analysis of ANKRD1 in nucleus of HL-1 cells with ISO and ivermectin treatments (n = 6). (G) Representative images and quantitative analysis of NRVMs area stained by α-actinin under the treatments of ISO and ivermectin (n = 6). (H) Representative images and quantitative analysis of NRVMs area with ANKRD1 knockdown (n = 6). (I) Echocardiographic analysis of mice treated with ANPep (n = 6). (J) Western blotting analysis of ANKRD1 in nucleus of mice treated with ANPep. One-way ANOVA with the Tukey post-test was used for comparisons.

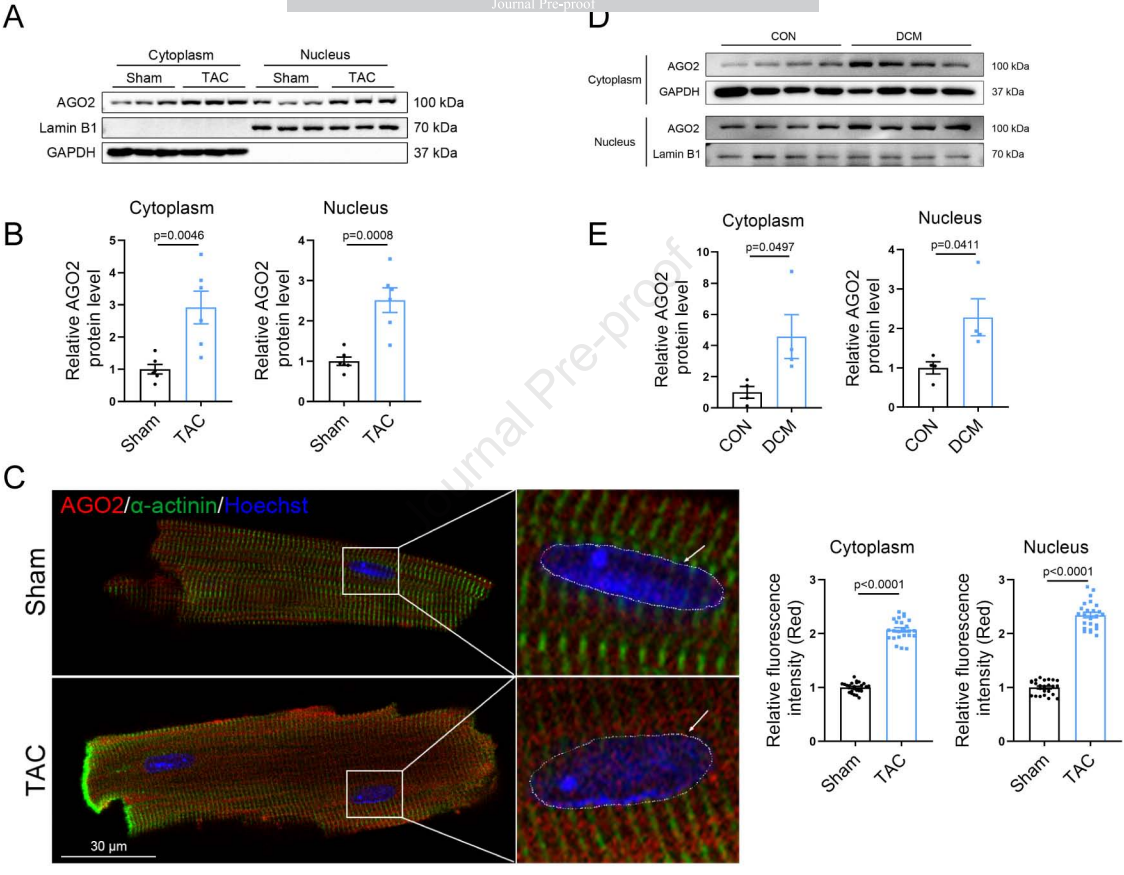

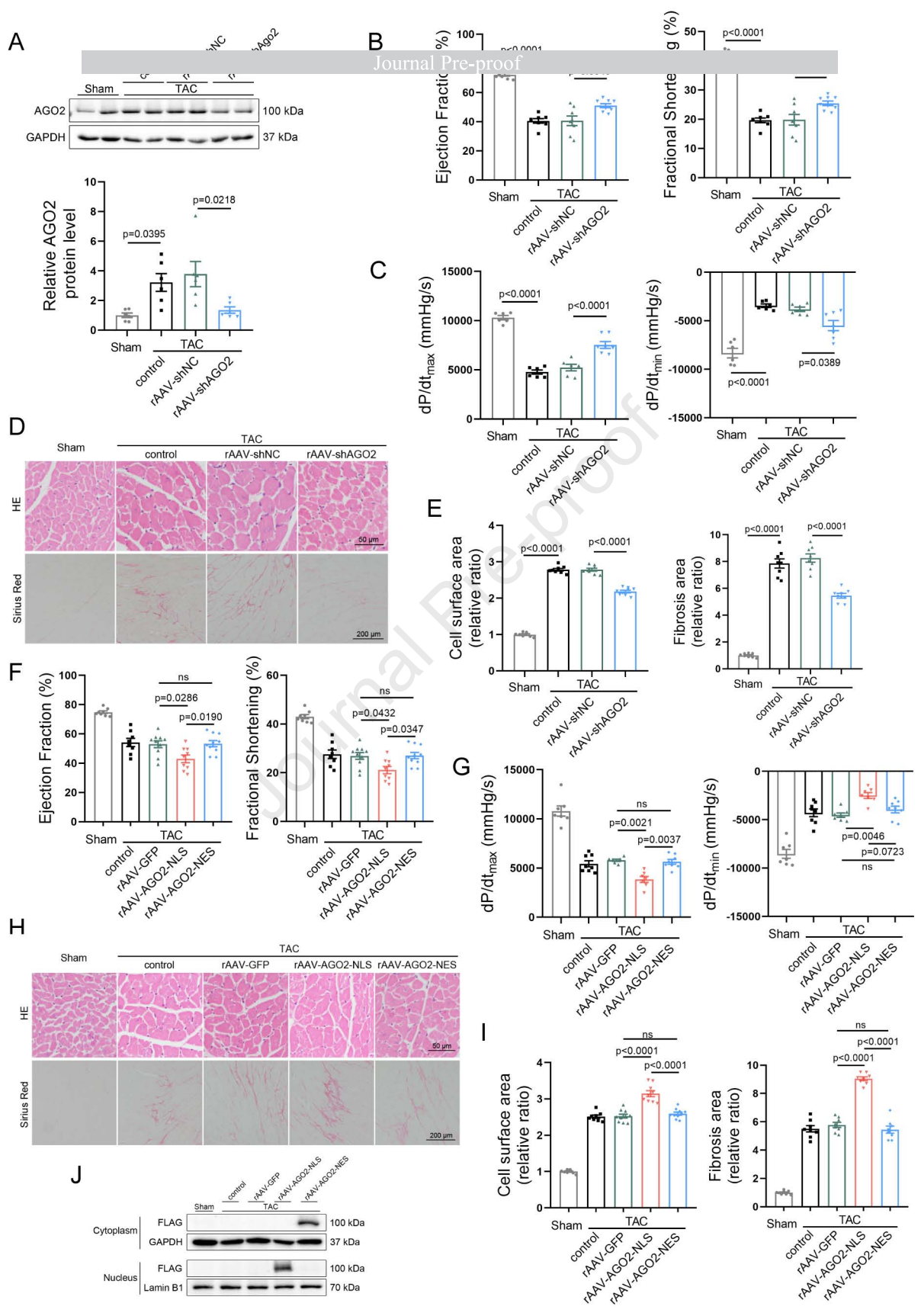

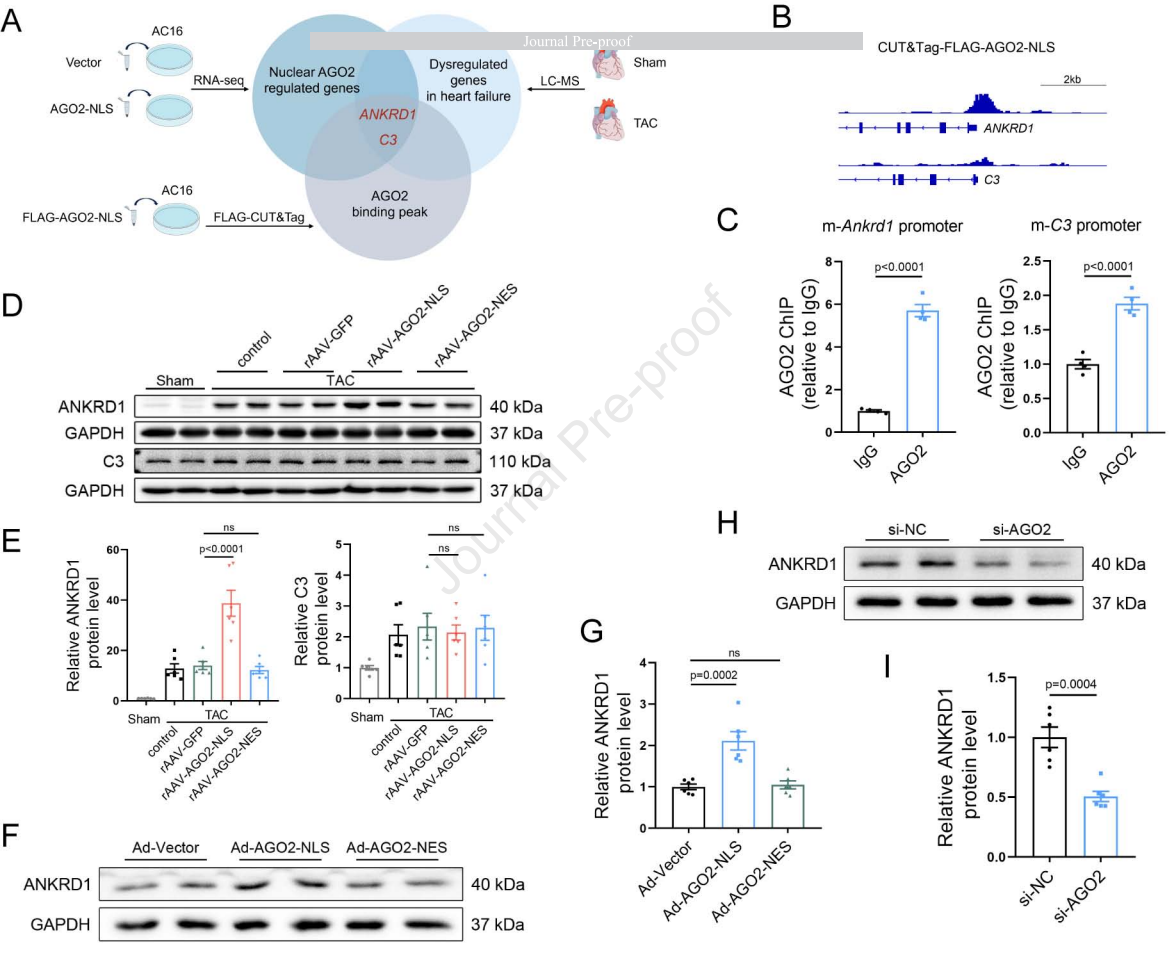

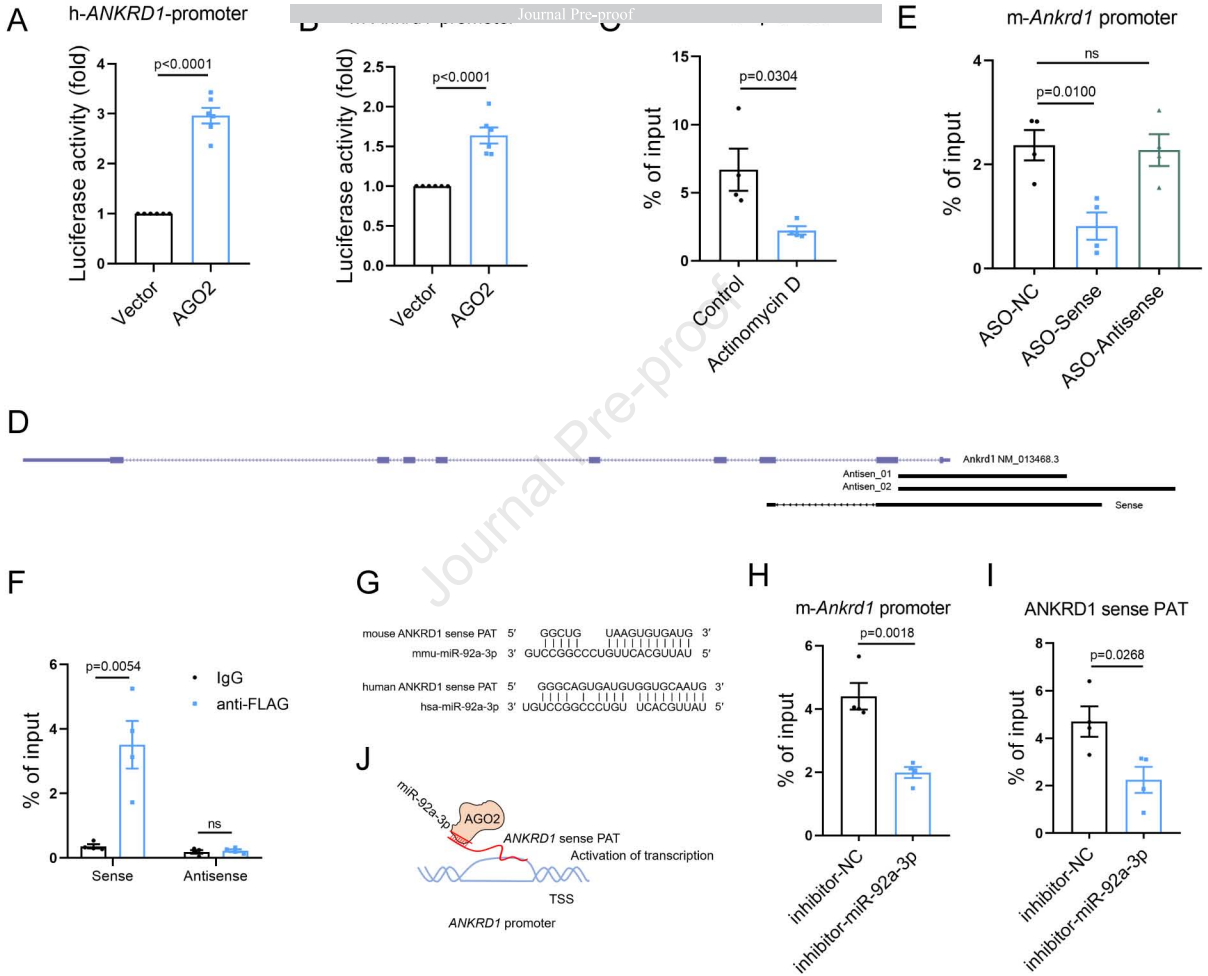

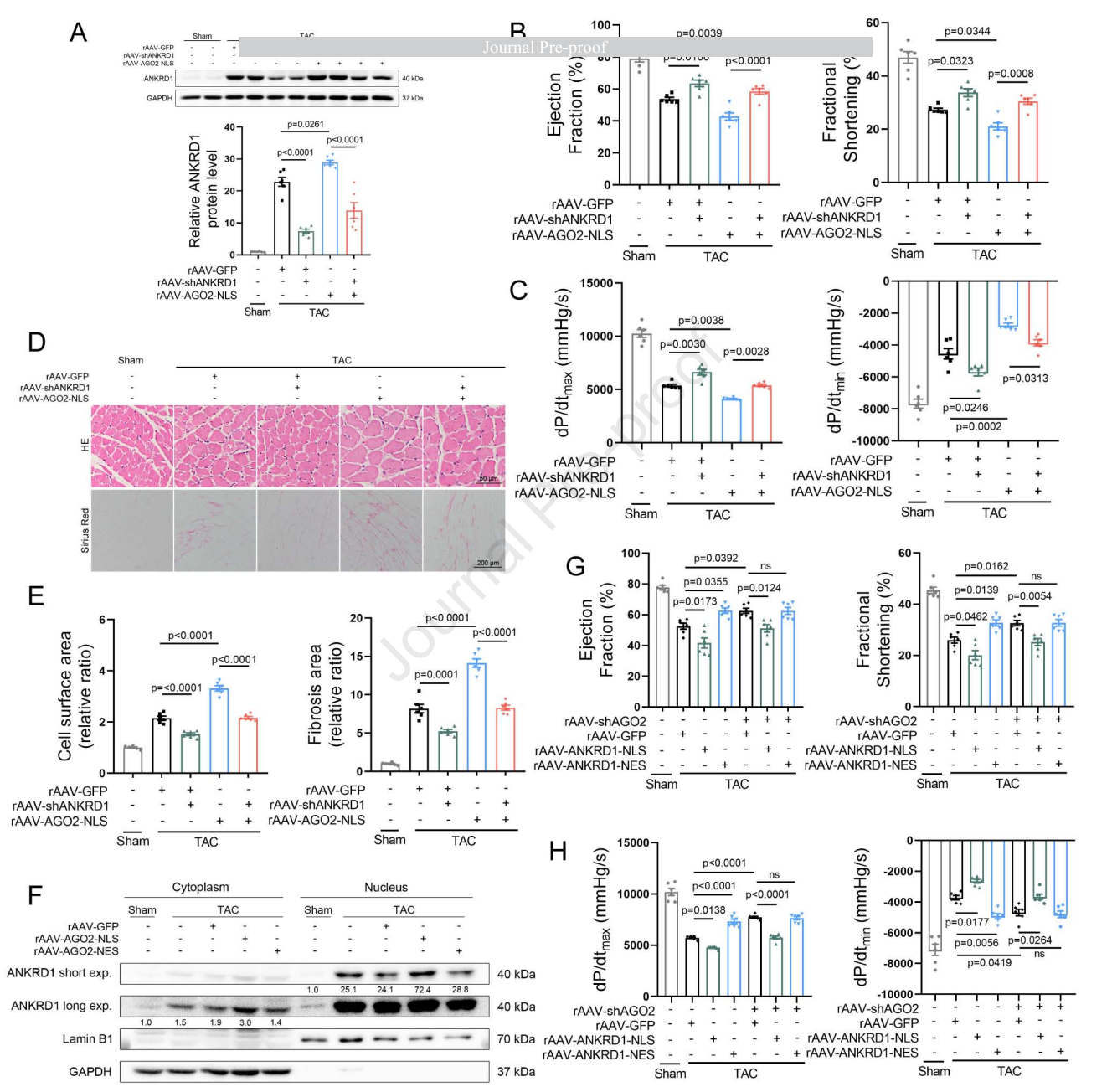

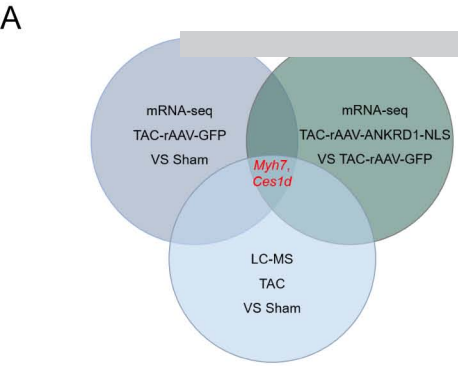

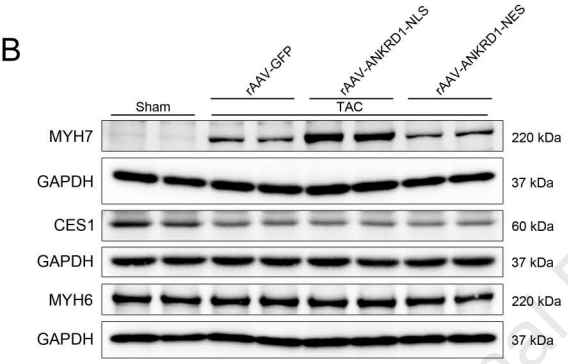

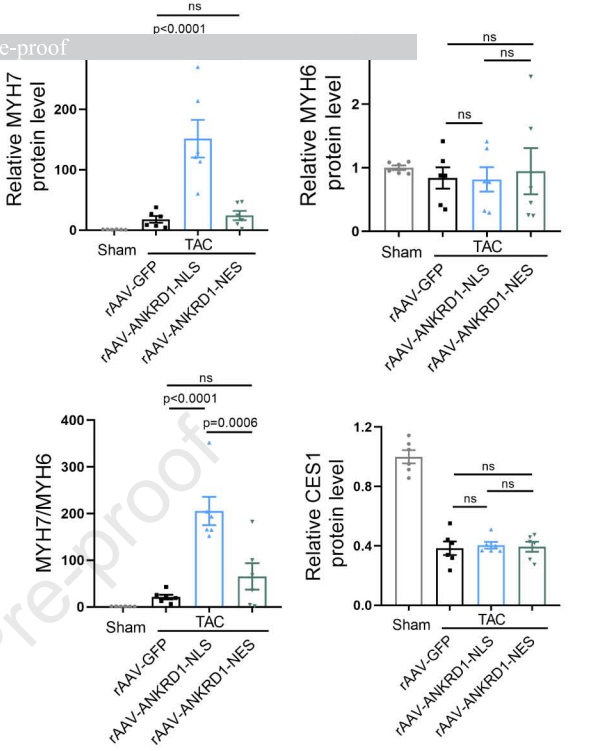

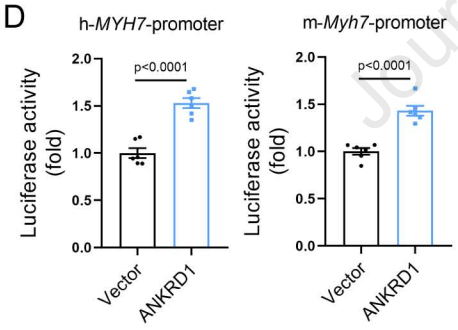

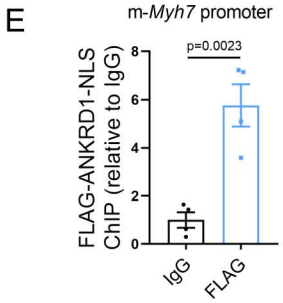

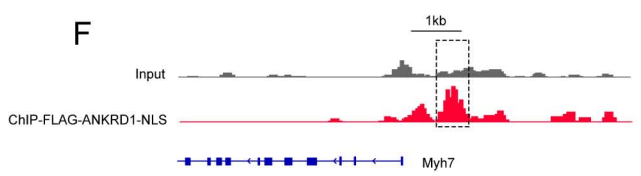

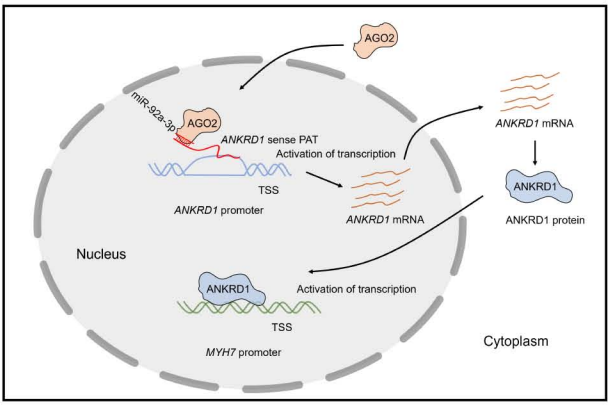

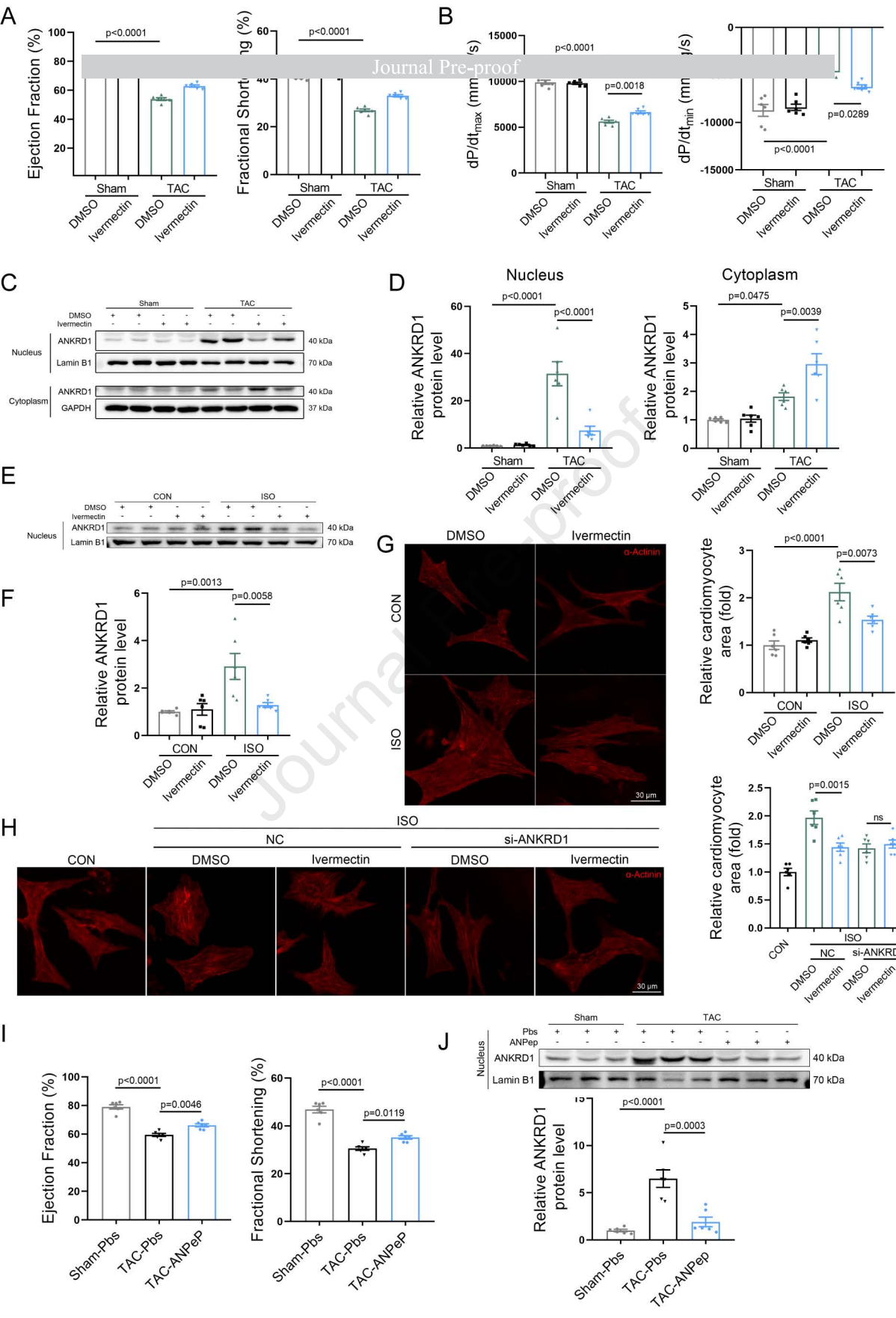

Li and colleagues find that nuclear AGO2 is upregulated in pressure overload-induced failing hearts, which acts in the nucleus to enhance *ANKRD1* transcription, and finally lead to cardiac remodeling. Importantly, AGO2-knockdown, ANKRD1-knockdown, and blockage of the ANKRD1 nuclear import can effectively rescue cardiac dysfunction in transverse aortic constriction-induced heart failure.